The IL32/BAFF axis supports prosurvival dialogs in the lymphoma ecosystem and is disrupted by NIK inhibition

Salomé Decombis, Antonin Papin, Céline Bellanger, Clara Sortais, Christelle Dousset, Yannick Le Bris, Thiphanie Riveron, Stéphanie Blandin, Philippe Hulin, Benoit Tessoulin, et al.

haematologica
Journal of The Ferrata Storti Foundation

The IL32/BAFF axis supports prosurvival dialogs in the lymphoma ecosystem and is disrupted by NIK inhibition

by Salomé Decombis, Antonin Papin, Céline Bellanger, Clara Sortais, Christelle Dousset, Yannick Le Bris, Thiphanie Riveron, Stéphanie Blandin, Philippe Hulin, Benoit Tessoulin, Mathieu Rouel, Steven Le Gouill, Agnès Moreau-Aubry, Catherine Pellat-Deceunynck, and David Chiron

Received: August 11, 2021.
Accepted: February 9, 2022.

Citation: Salomé Decombis, Antonin Papin, Céline Bellanger, Clara Sortais, Christelle Dousset, Yannick Le Bris, Thiphanie Riveron, Stéphanie Blandin, Philippe Hulin, Benoit Tessoulin, Mathieu Rouel, Steven Le Gouill, Agnès Moreau-Aubry, Catherine Pellat-Deceunynck, and David Chiron. The IL32/BAFF axis supports prosurvival dialogs in the lymphoma ecosystem and is disrupted by NIK inhibition.
Haematologica. 2022 Mar 10. doi: 10.3324/haematol.2021.279800. [Epub ahead of print]

The IL32/BAFF axis supports prosurvival dialogs in the lymphoma ecosystem and is disrupted by NIK inhibition

Salomé Decombis[1,2,3], Antonin Papin[1,2,3], Céline Bellanger[1,2,3], Clara Sortais[1,2,3,4], Christelle Dousset[1,2,3,4], Yannick Le Bris[1,2,3,5], Thiphanie Riveron[1,2,3], Stéphanie Blandin[6], Philippe Hulin[6], Benoit Tessoulin[1,2,3,4], Mathieu Rouel[1,2,3], Steven Le Gouill[1,2,3,4], Agnès Moreau-Aubry[1,2,3], Catherine Pellat-Deceunynck[1,2,3] and David Chiron[1,2,3,*]

[1] Nantes Université, Inserm, CNRS, Université d'Angers, CRCI2NA, Nantes - France
[2] L'Héma-NexT, i-Site NexT, Nantes, France
[3] GDR3697 Micronit, CNRS
[4] Service d'Hématologie Clinique, Unité d'Investigation Clinique, CHU, Nantes, France.
[5] Service d'Hématologie Biologique, CHU, Nantes, France
[6] SFR-Santé, INSERM UMS016, CNRS UMS 3556, FED 4202, UNIV Nantes, CHU, Nantes, France

* Corresponding author:

Tel: +33 228080297

Address: 8 quai Moncousu, 44007 Nantes, France

E-mail: david.chiron@univ-nantes.fr

Acknowledgements: The authors thank la Ligue Contre le Cancer Grand-Ouest, i-Site NexT (ANR-16-IDEX-0007), the SIRIC ILIAD (INCa-DGOS-Inserm_12558), ERRATA (Région Pays de la Loire program 2015-2018) and Actions Cancer 44. CS is the recipient for a fellowship from Plan Cancer (FRFT). MicroPICell facility is a member of the national infrastructure France-BioImaging supported by the French National Research Agency (ANR-10-INBS-04). The authors thank Dr. Martine Amiot for her critical review of the manuscript. The authors are also most grateful to the Genomics and Bioinformatics Core Facility of Nantes (GenoBiRD, Biogenouest, IFB) and the flow cytometry core facility (Cytocell, SFR Bonamy) for their technical support.

Author contributions: SD and AP designed and performed experiments and analyzed data. CB performed experiments and participated in bioinformatics. CS, CD, TR, AMA and YLB performed experiments and analyzed data. BT and MR participated in bioinformatics analysis. SB and PH participated in IHC experiments and analysis. SLG participated in the design of the study. CPD participated in the design of the study, in the data analysis, and in the writing of the article. DC designed the study, performed experiments, analyzed data, and wrote the article.

Availability of data and materials: All RNA-seq datasets are publicly available in GEO. All other datasets analyzed during the current study are available from the corresponding author on reasonable request.

Conflict of interest: The authors declare that they have no conflict of interest.

Running Title: MCL protumoral ecosystem

The manuscript contains 8 Figures, 9 supplementary figures and 3 supplementary tables

Abstract:

Aggressive B-cell malignancies, such as mantle cell lymphoma (MCL), are microenvironment-dependent tumors and a better understanding of the dialogs occurring in lymphoma protective ecosystems will provide new perspectives to increase treatment efficiency. To identify novel molecular regulations, we performed a transcriptomic analysis based on the comparison of circulating (n=77) versus MCL lymph nodes (n=107) together with RNA sequencing of malignant (n=8) versus normal B-cell (n=6) samples. This integrated analysis led to the discovery of microenvironment-dependent and tumor-specific secretion of the interleukin-32 beta (IL32β), whose expression was confirmed *in situ* within MCL lymph nodes by multiplex immunohistochemistry. Using *ex vivo* models of primary MCL cells (n=23), we demonstrated that, through the secretion of IL32β, the tumor was able to polarize monocytes into specific MCL-associated macrophages, which in turn favor tumor survival. We highlighted that while IL32β-stimulated macrophages secreted several protumoral factors, they supported tumor survival through a soluble dialog, mostly driven by BAFF. Finally, we demonstrated the efficacy of selective NIK/alternative-NFκB inhibition to counteract microenvironment-dependent induction of IL32β and BAFF-dependent survival of MCL cells. This data uncovered the IL32β/BAFF axis as a previously undescribed pathway involved in lymphoma-associated macrophages polarization and tumor survival, which could be counteracted through selective NIK inhibition.

Key words: IL32, BAFF, Mantle Cell Lymphoma, macrophages, NIK

Introduction:

While most studies have focused on tumor cells for years, allowing the discovery of numerous key (epi)-genetic aberrations and oncogenic pathways, it is now widely accepted that ecosystem integration is also critical for the understanding of cancer progression. Evidence demonstrating that the tumor ecosystem plays a central role in tumoral expansion and treatment resistance has continued to accumulate since the emergence of the tumor microenvironment (TME) concept more than a century ago[1]. Indeed, the tumor ecosystem has shown multiple facets, from its critical role in cancer metabolism to the influence of mechanical constraints, not to mention the diversity of immune infiltrates[2]. A better understanding of TME now supports the development of next generation therapeutic strategies, such as rational targeted therapy combinations to bypass microenvironment-dependent resistance[3], immune checkpoint inhibitors and bi-specific antibodies[4].

Mantle cell lymphoma (MCL) is a rare and mostly incurable B-cell malignancy and strategies to overcome resistance and treat MCL relapses are an unmet medical need[5]. Over the past decades, most studies have focused on structural and functional genomic anomalies which have led to important discoveries regarding MCL's molecular origin (i.e. t(11;14)), factors involved in the highly heterogeneous clinical course of this disease (i.e. *SOX11*, *TP53*, *CDKN2A*)[6-8], as well as markers of drug resistance[9-11]. In contrast to tumoral intrinsic anomalies, the dialog between MCL and its TME was largely ignored. Nevertheless, we, and others, have suggested a dynamic dialog within lymph nodes, which are the MCL's primary expansion zones. MCL cells are able to shape their microenvironment[12], whereas the latter is necessary to trigger cell cycle activation[13], apoptosis inhibition and drug resistance[14] as well as oncogenic pathways activation, such as NFκB and BCR pathways[15]. These findings confirmed the need to consider the biology of the TME in MCL and encourage further studies to understand the complexity of its dialogs and the supporting molecular regulations.

Unlike other B-cell lymphomas, MCL is characterized, as promptly as on diagnosis, by early dissemination in virtually all patients, with a significant number of circulating lymphoma cells, mostly in the bone marrow (BM) and peripheral blood (PB)[16]. This characteristic allows the comparison of tumor cells within several organs and the identification of regulations specifically induced in the lymphoid niches. To identify TME-dependent molecular regulations in MCL, we first performed a global unbiased transcriptomic analysis integrating samples from PB and LN tissue and cells from *ex vivo* models. Our analysis uncovered the microenvironment-dependent and tumor-specific expression of interleukine-32 (IL32), a soluble factor whose role in lymphomas is unknown. We showed that tumor-specific IL32 plays a major role in the corruption of the immune ecosystem that supports MCL survival and identified druggable therapeutic targets involved in these interplays.

Methods:

Primary cells culture

MCL cells were obtained after informed consent from patients according to protocols approved by local institutional review boards (REFRACT-LYMA cohort; ethical approval GNEGS-2015-09-13[17]) and in accordance with the Declaration of Helsinki. Patients' characteristics are summarized in supplemental Table S1. For comparison with normal naive CD5+ B cells (NBC), cord blood B cells were isolated and cultured using the same protocol. As previously described, MCL and NBC were cultured with growth factors (IL10: 50 ng/mL, BAFF: 50 ng/mL, IGF1: 10 ng/mL, IL6: 1 ng/mL) on adherent CD40L-expressing fibroblasts previously treated with mitomycin-C[13]. The ratio of adherent cells and MCL cells was 1/10.

PB was obtained from age-matched (>60 years) healthy donors. Monocytes were obtained by elutriation and T cells were separated using anti-human CD3 magnetic beads. *In vitro* generation of M1 and M2-10 monocyte-derived macrophages (Mϕ) was performed as previously described[12]. Regarding Mϕ-32, monocytes were differentiated with CSF1 (M-CSF, 50 ng/mL, 5 days) before activation with recombinant human (rh)IL32β (100 ng/mL, 2 days).

Bioinformatics analysis

Gene Expression Profiling (GEP). Publicly available datasets for MCL cells in lymph node (n=107) or peripheral blood (n=77) were collected from the GEO database (GSE70910, GSE16455, GSE21452, GSE35426, GSE36000, GSE124931 and GSE95405) and analyzed as previously described[14].

Full length RNA-seq. CD19+CD5+ MCL cells from PB (n=4) and CD19+CD5+ B cells from cord blood (NBC, n=3) were cultured *ex vivo* on CD40L-expressing fibroblasts with growth factors for 7 days[13]. RNA was sequenced at baseline (D0) and after 7 days of culture. "Tumor specific" and "Shared with NBC" genes were determined by comparing MCL cells transcriptome with the one of NBC. "Tumor specific" genes were found up-regulated in culture *ex vivo* and in LN *in vivo* but not in NBC samples.

3'seq-RNA Profiling[18]. Briefly, raw counts were normalized and transformed and differential gene expression was assessed with DESeq2 package in R. Similar results were obtained using EdgeR package in R. Principal component analysis (PCA) was performed by FactoMineR and factoextra packages. A hierarchical ascendant clustering was performed using Euclidean distances and Ward.D2 method. Heatmap was carried out with the ComplexHeatmap package.

All datasets have been deposited to GEO database (GSE179636 and GSE179766).

Multiplex Immunohistochemistry (IHC)

Formalin-fixed paraffin-embedded tissue sections were subjected to pretreatment involving antigen retrieval by heating in EDTA buffer at the beginning of the experiment and to a TR1 Retrieval between each staining. Tissue sections were then stained for Cyclin D1, IL32, CD68 and CD3 with polymer enhancer and HRP 2-Step polymer and the buffer 1X Plus Amplification Diluent with Opal 570, 650, 520 and 690 for the detection of Cyclin D1, IL32, CD68 and CD3 respectively. For the nucleus staining, we used DAPI (1:4000). The experiment was realized in the automated lmpath36. Images were acquired on a Nikon A1 RSi confocal fluorescence microscope with spectral module.

Additional methods are detailed in the supplemental Methods section and Table S2.

Results:

Microenvironment-dependent IL32 expression in MCL cells is tumor specific.

We first analyzed differential gene expression between unpaired MCL samples from lymph nodes (LN, n=107) and peripheral blood (PB, n=77): 6887 genes were differentially expressed (log2Fc>0.5 and <-0.5; adjusted p-value<0.05) suggesting a central role of the LN ecosystem in MCL transcriptional programs (Figure 1A). The 22 most differentially expressed genes (log2Fc>5 and <-5) were predicted to belong to the extracellular region (Figure S1A), and this was also highlighted by top functional annotations, including Extracellular Matrix-Receptor (ECM-R) interactions (hsa#04512), Cytokines-Cytokine Receptor interactions (hsa#04060) or Cell Adhesion Molecules (hsa#04514), reflecting active cellular communication between tumor cells and their ecosystems (Figure S1B).

Because LN sections used for gene expression profiling displayed heterogeneous tumor and immune cell infiltrations, we needed to perform additional analyses to identify MCL specific transcriptomic regulations. To this end, we compared transcriptomic data from LN with transcriptomic data from $CD19^+$ circulating MCL cells cultured on CD40L expressing cells (Figure 1B). This *ex vivo* culture model was designed to mimic signals occurring in the LN and was composed of CD40L-expressing cells complemented by several protumoral growth factors[13]. More than 70% of the genes upregulated *ex vivo* in the culture model were also overexpressed in LN as compared with MCL PB (n=3217/4524) (Figure 1B). Accordingly, MCL “LN signature” as well as previously described signatures enriched in MCL tissue, such as “NFκB”, “BCR” or “NIK”[15] , were significantly upregulated in the *ex vivo* culture model (Figure S1C).

By comparing the upregulated gene set (both up in LN and in culture, n=3217) with CD40L-stimulated CD5+ normal B-cells (NBC), we identified that 39% of the differentially expressed genes were tumor-specific (i.e., were not upregulated in NBC) (Figure 1B). Functional

annotations showed that the soluble dialog (hsa#04060) was specifically enriched in the tumor ecosystem, in contrast to ECM-R interactions or cell cycle activation, which were shared with NBC (Figure S1D). Top-genes scoring revealed that, respectively, *CCL22* and *IL32* were the most upregulated genes within "Shared with NBC" and "Tumor-specific" transcriptional programs (Figure 1C). While CCL22 production has been previously characterized as microenvironment-dependent in several B-cell malignancies[19], the mechanisms of regulation and the biological role of IL32 have remained unknown. Constitutive expression of IL32 in 3/9 cell lines first confirmed that MCL has indeed the ability to produce and secrete IL32 (Figure 1D, S2A). Finally, splicing analysis of RNA-seq data showed that the predominant isoform in MCL was IL32β (Figure S2B).

IL32 is expressed in MCL LN and is induced *in vitro* upon CD40 triggering

We showed that PB MCL displayed a slight, but significant, overexpression of IL32 when compared to NBC, and high expression was observed in most LN MCL studied (Figure 2A). IL32 induction in LN was confirmed in paired samples both at the RNA (n=8) and protein (n=3) levels (Figure 2B). Consistently with our observation in cell lines, constitutive RNA expression was detected in 24% of PB MCL samples (5 out of 21), independently of p53 status or disease subtype (Table S1). CD40L induced IL32 expression in 10 out of 13 MCL samples but not in NBC (Figure 2C-D). Of note, the 3 samples in which IL32 induction was not detected were all from the indolent leukemic non-nodal subtypes of MCL. A similar CD40-dependent induction of IL32 was observed in MCL cell lines (Figure S2C-D).

To further characterize the pattern of IL32 expression *in situ*, we performed immunohistochemistry (IHC) on 4 MCL tissue samples. Figure 3A shows IL32+ cells in 4 out of 4 MCL samples. We further used IHC multiplex in two samples for the concurrent detection of MCL cells (Cyclin D1), macrophages (CD68), T cells (CD3) and IL32. We observed that IL32 expression was enriched *in situ* in tumor zones infiltrated with T cells (ROI#1 and #2 of sample LN#2, ROI#1 of sample LN#3), compared to areas containing only

tumor cells (ROI#2 of LN#3) (Figure 3B,C). Taken together these results show that IL32 is expressed *in situ* by MCL cells in the vicinity of T-cells.

CD40L-dependent IL32 expression in MCL cells depends on alternative NFκB **pathway**

We next determined whether NFκB pathways controlled IL32 induction. CD40 triggers activation of both classical (ser32/34 IkBα phosphorylation, pIkB) and alternative (p52 increase) NFκB pathways (Figure 4A). Inhibition of IkB kinases IKK-1/2, using BMS-345541[20], dramatically reduced the activation of both NFκB pathways and resulted in the complete inhibition of IL32 (Figure S3A). However, siRNA against *NFKB1* failed to reduce IL32 expression in Mino cells (Figure S3B), suggesting that the classical NFκB pathway was not involved. To confirm the role of the alternative pathway, we used the NIK inhibitor SMI1, which was recently described as selectively inhibiting the alternative NFκB pathway[21]. NIK-i, which inhibited p52 processing from p100 without inducing any modulation of pIkB, resulted in the inhibition of both constitutive (Mino) and CD40L-induced (NTS3, REC1 and primary MCL) IL32 (Figure 4B,C). Of note, the detection of high p52 expression in LN tissue further confirmed the activation of an alternative NFκB pathway *in vivo* (Figure S3C). Nevertheless, even though IL32 induction was restricted to tumor cells, activation of alternative NFκB pathway was observed in both NBC and MCL cells upon CD40 triggering (Figure 4D). Moreover, p52 constitutive cell lines did not necessarily expressed IL32 (Figure 4E), suggesting that the alternative NFκB pathway may not be sufficient for IL32 induction and leading us to investigate another layer of regulation.

***IL32* is hypomethylated in MCL cells**

We wondered whether IL32 locus could be also epigenetically regulated. Indeed, decitabine induced IL32 expression in IL32-negative MCL cells (Figure S4A). Bisulfite sequencing showed that IL32-positive and negative MCL cells displayed a significantly different methylation pattern in both promoter and CpG island of *IL32* gene locus (40.5% vs. 73% and

24% vs. 97 %, respectively), suggesting that hypomethylation favored IL32 expression (Figure S4B). Similarly, IL32 promoter was hypermethylated in NBC compared to MCL cells (100% vs. 40.5 %, respectively) and this pattern remained stable even after NBC stimulation with CD40L (Figure S4C,D). Collectively our data argued for epigenetic-driven expression of IL32 explaining the tumor-restricted expression.

Myeloid cells strongly respond to IL32

We next decided to assess the biological consequences of IL32β production within the MCL ecosystem. We first addressed the role of recombinant human (rh)IL32β on the tumor itself, but did not observe any changes, neither on MCL cell survival and proliferation *ex vivo* nor on previously-described IL32-induced signaling pathways and expression of protumoral factors[22] (Figure 5A,B and data not shown).

As IL32 receptor has yet to be identified, we performed functional annotations of IL-32 co-regulated genes within lymphoma LN to decipher the cell types that could respond to MCL-produced IL32β. We observed enrichment in pathways such as phagosome (hsa#04145), chemokine (hsa#04062) or Th17 differentiation (hsa#04659), suggesting myeloid and T-cell involvement in MCL-related IL32β functions (Figure S5A). In addition, top *IL32* co-regulated genes were enriched with key regulators of macrophage function as well as the T-cell related marker CD2 (adjusted $p<0.0001$) (Figure S5B). Consistently, the induction of STAT3 phosphorylation on tyr705 (pSTAT3) in both cell types confirmed their ability to respond to IL32, with monocytes also displaying additional induction of NFκB pathways (Figure 5C). We next analyzed the transcriptome of rhIL32β-stimulated monocytes (Mono, n=3), monocyte-derived macrophages (Mϕ, n=3) and T-cells (T, n=3). As shown in the PCA, IL32β greatly modulated both monocytes and Mϕ, but only slightly the T-cell transcriptomes (Figure 5D). Consistently, hierarchical clustering was able to discriminate myeloid cells according to IL32β stimulation by not T cells (Figure 5E).

We then focused on common modulations and their resulting functional annotations, arising from IL32β-stimulated monocytes and Mϕ (Figure S5C,D). Consistent with the activation of STAT3 and NFκB pathways at the protein level (Figure 5C), we observed a significant enrichment in JAK-STAT (hsa#04630) and NF-kB (hsa#04064) pathways (Figure S5D). In addition, enrichment of several pathways related to soluble factors, such as IL17 (hsa#04657), TNF (hsa#04668), chemokine and cytokine signaling (hsa#04062, hsa#04060), suggested that IL32β might regulate the secretome of monocyte/Mϕ (Figure S5D). Taken altogether these results suggested that IL32β secreted by MCL in its ecosystem would result in the stimulation of monocyte/Mϕ and potentially influence their secretome.

MCL-secreted IL32β led to specific differentiation of monocytes into protumoral CD163+ macrophages (Mϕ-32)

To determine the nature of secretome modifications in monocyte/macrophages stimulated by IL32β, we further focused our analysis on a list of 370 cytokines and chemokines (annotated in GO#0008009 and #0005125). Among them 108 were expressed in at least one sample and many of them were induced after IL32β stimulation in monocytes (n=48) or macrophages (n=40) (Figure 6A). Most of these modulations were observed in both monocytes and macrophages (n=29) and were validated by RT-qPCR and cytokine array (Figure S6).

To confirm these results with MCL-secreted IL32β, we generated IL32$^{-/-}$ MINO cells (Figure S7A,B) and evaluated the ability of their supernatant to induce the validated rhIL32β-modulated genes on monocyte/macrophages (*IL1A*, *IL1B*, *IL6*, *IL24*, *CXCL8*, *TNFSF13B, IL32)*. As expected, IL32$^{-/-}$ MINO supernatant was characterized by a lesser ability to induce these genes in monocyte/macrophages compared to IL32$^{+/+}$ cells (Figure 6B). These results were confirmed with CD40L-stimulated IL32$^{-/-}$ NTS3 cells (Figure S7C).

Using previously published macrophage subtype characterization[12], we determined that IL32β-induced soluble factors were associated to both M1-like (53%) and M2-like (47%) secretomes. We have recently described such a dual M1/M2 profile in MCL-associated macrophages (Mϕ-MCL) and accordingly 85% of IL32β-induced factors were found expressed by Mϕ-MCL (Figure 6C)[12]. In addition, Mϕ-32 displayed similar $CD163^{mid}$ expression, a marker of protumoral macrophages, which we previously described regarding Mϕ-MCL (Figure 6D). Finally, we confirmed, using culture inserts, that the Mϕ-32 secretome was protumoral, inducing a 3-fold increase in MCL cell survival compare to MCL cells alone (median survival 12.5%; versus 38%; $p < 0.01$; Figure 6E).

Collectively these results showed that monocytes/macrophages responded to MCL-secreted IL32β, resulting in their polarization into protumoral $CD163^{mid}$ Mϕ-32 expressing both M1 and M2-associated secretome, which were similar to Mϕ-MCL.

BAFF is involved in Mϕ-32 prosurvival dialog through activation of alternative NFκB in MCL cells

Lastly, we aimed to uncover the factors involved in the prosurvival soluble dialog between Mϕ-32 and MCL cells. We first tested a panel of 9 growth factors induced by IL32β for their capacity to support long-term (7 days) survival of MCL cells (Figure 7A). Remarkably, only BAFF was able to support MCL-cell survival alone (n=9) at a level similar to Mϕ-32 supernatant (s_ Mϕ-32) (Figure 7B).

BAFF binds to three receptors, BAFF-R, TACI and BCMA, the last two being shared with the growth factor APRIL. In contrast to BAFF, APRIL did not support MCL survival (Figure 7B), suggesting that TACI and BCMA were not involved in the protumoral dialog studied here. We showed that most MCL cells highly expressed BAFFR and that *TNFSF13B* expression was enriched in MCL LN when compared to PB ($p<0.0001$), suggesting a key role of this growth factor in MCL tissue (Figure S8A,B). We also confirmed that Mϕ-32 were able to secrete a significant amount of BAFF, in contrast to MCL (Figure 7C), and showed that rhBAFF

induced the selective activation of the alternative NFκB pathway in MCL cells and cell lines (processing of p52, Figure S8C). Accordingly, NIK-i was able to counteract the survival support provided by rhBAFF in MCL cells (median reduction of 95%, n=4, $p<0.05$, Figure S8D). NIK-i also reduced the survival support provided by s_Mϕ-32, with a median reduction of 47% (n=6, $p<0.05$) and almost entirely in 3 out of 6 samples, suggesting an involvement of BAFF in s_Mϕ-32 (Figure 7D). Indeed, in these NIK-i sensitive samples, BAFFR-neutralizing antibodies resulted in the inhibition of s_Mϕ-32 protumoral support with a level similar to NIK-i (Figure 7E). Accordingly, s_Mϕ-32 resulted in the activation of the alternative NFκB pathway, which was counteracted using BAFF/BAFF-R-neutralizing antibodies (Figure 7F, S8E). Taken together, these data showed that BAFF secreted by Mϕ-32 was involved in the protumoral dialog with MCL, which can be counteracted by selective NIK-i or BAFFR-neutralizing antibodies.

Discussion:

IL32 is a newly characterized cytokine composed of seven variants, generated by alternative splicing, with differential biological roles[23,24]. IL32α, IL32β and IL32γ are the isoforms which have been studied the most up to now, IL32β being the most frequently expressed in cancer[25], as shown here for MCL. The putative receptor for IL-32 is unknown and the lack of IL32 expression in rodents considerably limits our knowledge on its physiological roles. Nevertheless, IL-32β expression has been documented in several solid cancers and seems to be involved in many biological processes such as migration, metastasis, proliferation, and apoptosis[25]. We have shown here that IL32β, which was secreted by lymphoma cells, did not directly increase tumor cell survival, but participated in the tumor-specific shaping of macrophages. Such a paracrine role of IL32 has been recently described in multiple myeloma, a plasma cell neoplasm[26], reinforcing the critical role of this soluble factor in the ecosystem of B-cell malignancies.

Whereas IL32 was initially characterized for its pro-inflammatory properties[27], recent studies have highlighted that IL32 was preferentially expressed in regulatory T-cells in the bone marrow[28] and that it was able to promote immunoregulatory responses, especially through the induction of IL10 or IDO by macrophages[29-31]. Here we have confirmed, through a transcriptomic analysis of IL32β–induced genes in monocyte/macrophages, the ability of IL32β to induce the production of both pro- (e.g. IL6, OSM, IL1a, IL1b) and anti- inflammatory (e.g. IL10, IDO, IL18, IL4L1, CCL22)[19,32,33] soluble factors (Figure 5).

We have recently published that, through soluble interplay, MCL polarizes monocytes into tumor-specific macrophages (Mϕ-MCL), which in turn favors tumor survival[12]. We have demonstrated that Mϕ-MCL express both pro- (M1) and anti- (M2) inflammatory associated secretome, suggesting that factors other than classical M2-polarizing factors (such as MCL-secreted IL-10 and CSF-1) might be involved in Mϕ-MCL phenotype. Herein, we have found that MCL-secreted IL32β is most likely to be involved in this specific MCL-associated macrophage profile, most of these M1 and M2-like factors being common to both Mϕ-MCL and Mϕ-32. In addition, Mϕ-32 shares Mϕ-MCL phenotypical and functional characteristics i.e., $CD163^{mid}$ expression or MCL survival support through soluble dialog, respectively (Figure 6). Only a few studies have addressed the crosstalk between tumor-associated macrophages and MCL cells, so far[12,34,35]. Of note, a recent publication has highlighted that LN infiltrating CD163+ MCL-associated macrophages correlates to a poor prognosis in MCL[36], suggesting that targeting this interplay could be an interesting perspective for novel therapeutic options.

Among IL32β-induced secretomes, several of them have been previously described as being involved in MCL expansion, such as IL6, IL10, BAFF or WNT5A[37-40]. Nevertheless, we have shown that only BAFF supported the long-term survival of MCL cells alone, at a level similar as that observed with the Mϕ-32 supernatant. Although BAFF is a well-described survival and growth factor for both normal and malignant B-cells[39], only a few publications have addressed the functional consequences of BAFF stimulation in MCL[41]. We have shown that

most MCL samples displayed an expression of BAFF receptor (BAFF-R), its activation leading to the selective processing of the alternative NFκB pathway (Figure 7). Of note, Medina and colleagues previously demonstrated that MSC-dependent MCL survival was also mediated by BAFF, suggesting a central role of this growth factor in MCL ecosystems[42]. Neutralizing antibodies are available for targeting either BAFF (Belimumab) or BAFF-R (VAY-736), both of which display interesting preclinical activity in B-cell malignancies such as CLL, alone or in combination with BTK inhibitors[43,44].

Our results highlight a major role of the alternative NFκB pathway in the interplay between CD40-activated MCL cells and macrophages, especially through the IL32/BAFF axis. Saba and colleagues highlighted that a so-called "NIK signature", reflecting the activity of alternative NFκB, was enriched in MCL LN tissue compared to PB[15]. Consistent with these results, we previously demonstrated strong processing of p52 in our CD40L culture model designed to mimic signals occurring within the LN[13]. Here we have confirmed that MCL cells cultured in this model are also characterized by the NIK signature (Figure S1). The alternative NFκB pathway is frequently constitutively activated in MCL by intrinsic anomalies in several key actors of this pathway, such as *MAP3K14* (coding for NIK), *TRAF2*, *BIRC3* or *TRAF3*[45]. In this present work, we have shown that alternative NFκB pathway activation is also able to influence the MCL ecosystem through microenvironment-dependent and tumor-specific IL32 induction and consecutive macrophage (re)programming. Thus, the alternative NFκB activation can be the consequence of both intrinsic anomalies and microenvironment interactions, highlighting a central role of this pathway, which appeared to be involved in drug resistance. Indeed, Rahal and colleagues showed that its constitutive activity was involved in ibrutinib resistance in MCL cell lines[11].

We previously demonstrated that CD40L-dependent survival was associated to an NFκB-dependent unbalance of the Bcl-2 family in MCL, including dramatic inductions of anti-apoptotic proteins such as BCLxL[13,14]. Even though BAFF is a well-described pro-survival factor, the precise molecular mechanisms involved in BAFF-dependent survival remain elusive and cell-type dependent[46,47]. In contrast to CD40L, BAFF did not induce BCLxL or

MCL1 in MCL cells and only a transitory increase of BCL2A1 was detected in cell lines (Figure S8F-H). Taken together, our data suggest that complementary protumoral pathways occur within the ecosystem. Further studies, such as modulations of Bcl2-family complexes at the mitochondrial level and characterization of the mitochondrial priming upon BAFF stimulation, are now necessary to decipher the molecular mechanisms involved in BAFF/ NFκB2 dependent regulation of apoptosis in MCL.

The specific inhibition of the alternative NFκB pathway was barely achievable until the very recent development of specific NIK inhibitors[21,48]. NIK is a kinase selectively involved in the alternative pathway by activating IKKa, which in turn induces the cleavage of p100 to p52, without affecting the canonical pathway. Here, we have confirmed the efficacy of NIK inhibition in counteracting microenvironment-dependent induction of IL32 (Figure 4) and BAFF-dependent survival of MCL cells (Figure 7). The central role of NFκB pathways in mature B cell malignancies is well-documented[49,50], reinforcing the strong rational to specifically target this pathway. Further development of molecules that selectively target key actors of alternative NFκB pathway (i.e. NIK, RELB) as well as their evaluation in early phase clinical trials are now needed to address their potential therapeutic value.

In summary, our data uncovered the IL32β/BAFF axis in MCL-associated macrophage polarization and tumor survival. Our data shows that targeting IL32β, BAFF or the alternative NFκB pathway could be of major interest for counteracting the multiple cross-talks that occur in the MCL microenvironment and, especially, the $CD40L^+$ T-cell / MCL / $CD163^+$ MCL-associated macrophage triad (Figure 8).

References

1. Maman S, Witz IP. A history of exploring cancer in context. Nat Rev Cancer. 2018;18(6):359-376.
2. Jin M-Z, Jin W-L. The updated landscape of tumor microenvironment and drug repurposing. Signal Transduct Target Ther. 2020;5(1):1-16.
3. Le Gouill S, Morschhauser F, Chiron D, et al. Ibrutinib, Obinutuzumab And Venetoclax In Relapsed and Untreated Patients with Mantle-Cell Lymphoma, a phase I/II trial. Blood. 2020;137(7):877.
4. Pytlik R, Polgarova K, Karolova J, Klener P. Current Immunotherapy Approaches in Non-Hodgkin Lymphomas. Vaccines. 2020;8(4):708.
5. Campo E, Rule S. Mantle cell lymphoma: evolving management strategies. Blood. 2015;125(1):48-55.
6. Delfau-Larue M-H, Klapper W, Berger F, et al. High-dose cytarabine does not overcome the adverse prognostic value of CDKN2A and TP53 deletions in mantle cell lymphoma. Blood. 2015;126(5):604-611.
7. Eskelund CW, Dahl C, Hansen JW, et al. TP53 mutations identify younger mantle cell lymphoma patients who do not benefit from intensive chemoimmunotherapy. Blood. 2017;130(17):1903-1910.
8. Nadeu F, Martin-Garcia D, Clot G, et al. Genomic and epigenomic insights into the origin, pathogenesis, and clinical behavior of mantle cell lymphoma subtypes. Blood. 2020;136(12):1419-1432.
9. Agarwal R, Chan Y-C, Tam CS, et al. Dynamic molecular monitoring reveals that SWI–SNF mutations mediate resistance to ibrutinib plus venetoclax in mantle cell lymphoma. Nat Med. 2019;25(1):119-129.
10. Chiron D, Di Liberto M, Martin P, et al. Cell-cycle reprogramming for PI3K inhibition overrides a relapse-specific C481S BTK mutation revealed by longitudinal functional genomics in mantle cell lymphoma. Cancer Discov. 2014;4(9):1022-1035.
11. Rahal R, Frick M, Romero R, et al. Pharmacological and genomic profiling identifies NF-κB–targeted treatment strategies for mantle cell lymphoma. Nat Med. 2014;20(1):87-92.
12. Papin A, Tessoulin B, Bellanger C, et al. CSF1R and BTK inhibitions as novel strategies to disrupt the dialog between mantle cell lymphoma and macrophages. Leukemia. 2019;33(10):2442-2453.
13. Chiron D, Bellanger C, Papin A, et al. Rational targeted therapies to overcome microenvironment-dependent expansion of mantle cell lymphoma. Blood. 2016;128(24):2808-2818.
14. Tessoulin B, Papin A, Gomez-Bougie P, et al. BCL2-Family Dysregulation in B-Cell Malignancies: From Gene Expression Regulation to a Targeted Therapy Biomarker. Front Oncol. 2018;8:645.
15. Saba NS, Liu D, Herman SE, et al. Pathogenic role of B-cell receptor signaling and canonical NF-κB activation in mantle cell lymphoma. Blood. 2016;128(1):82-92.
16. Ferrer A, Salaverria I, Bosch F, et al. Leukemic involvement is a common feature in mantle cell lymphoma. Cancer. 2007;109(12):2473-2480.
17. Hanf M, Chiron D, de Visme S, et al. The REFRACT-LYMA cohort study: a French observational prospective cohort study of patients with mantle cell lymphoma. BMC Cancer. 2016;16(1):802.
18. Charpentier E, Cornec M, Dumont S, et al. 3'RNA sequencing for robust and low-cost gene expression profiling. 2021 Jan 15. 10.21203/rs.3.pex-1336/v1. [Preprint]
19. Rawal S, Chu F, Zhang M, et al. Cross talk between follicular Th cells and tumor cells in human follicular lymphoma promotes immune evasion in the tumor microenvironment. J Immunol. 2013;190(12):6681-6693.
20. Burke JR, Pattoli MA, Gregor KR, et al. BMS-345541 is a highly selective inhibitor of IκB kinase that binds at an allosteric site of the enzyme and blocks NF-κB-dependent transcription in mice. J Biol Chem. 2003;278(3):1450-1456.
21. Brightbill HD, Suto E, Blaquiere N, et al. NF-κB inducing kinase is a therapeutic target for systemic lupus erythematosus. Nat Commun. 2018;9(1):1-14.

22. Sloot YJ, Smit JW, Joosten LA, Netea-Maier RT. Insights into the role of IL-32 in cancer. Semin Immunol. 2018:24-32.
23. Aass KR, Kastnes MH, Standal T. Molecular interactions and functions of IL□32. J Leuk Biol. 2021;109(1):143-159.
24. Sohn DH, Nguyen TT, Kim S, et al. Structural Characteristics of Seven IL-32 Variants. Immune Netw. 2019;19(2):e8.
25. Han S, Yang Y. Interleukin-32: Frenemy in cancer? BMB Rep. 2019;52(3):165.
26. Zahoor M, Westhrin M, Aass KR, et al. Hypoxia promotes IL-32 expression in myeloma cells, and high expression is associated with poor survival and bone loss. Blood Adv. 2017;1(27):2656-2666.
27. Kim S-H, Han S-Y, Azam T, Yoon D-Y, Dinarello CA. Interleukin-32: a cytokine and inducer of TNFα. Immunity. 2005;22(1):131-142.
28. Zavidij O, Haradhvala NJ, Mouhieddine TH, et al. Single-cell RNA sequencing reveals compromised immune microenvironment in precursor stages of multiple myeloma. Nat Cancer. 2020;1(5):493-506.
29. Kang JW, Choi SC, Cho MC, et al. A proinflammatory cytokine interleukin□32β promotes the production of an anti□inflammatory cytokine interleukin□10. Immunology. 2009;128(1pt2):e532-e540.
30. Smith AJ, Toledo CM, Wietgrefe SW, et al. The immunosuppressive role of IL-32 in lymphatic tissue during HIV-1 infection. J Immunol. 2011;186(11):6576-6584.
31. Yan H, Dong M, Liu X, et al. Multiple myeloma cell-derived IL-32γ increases the immunosuppressive function of macrophages by promoting indoleamine 2, 3-dioxygenase (IDO) expression. Cancer Lett. 2019;446:38-48.
32. Carbonnelle-Puscian A, Copie-Bergman C, Baia M, et al. The novel immunosuppressive enzyme IL4I1 is expressed by neoplastic cells of several B-cell lymphomas and by tumor-associated macrophages. Leukemia. 2009;23(5):952-960.
33. Nakamura K, Kassem S, Cleynen A, et al. Dysregulated IL-18 is a key driver of immunosuppression and a possible therapeutic target in the multiple myeloma microenvironment. Cancer Cell. 2018;33(4):634-648.
34. Song K, Herzog BH, Sheng M, et al. Lenalidomide inhibits lymphangiogenesis in preclinical models of mantle cell lymphoma. Cancer Res. 2013;73(24):7254-7264.
35. Le K, Sun J, Khawaja H, et al. Mantle cell lymphoma polarizes tumor-associated macrophages into M2-like macrophages, which in turn promote tumorigenesis. Blood Adv. 2021;5(14):2863-2878.
36. Rodrigues JM, Nikkarinen A, Hollander P, et al. Infiltration of CD163-, PD-L1- and FoxP3-positive cells adversely affects outcome in patients with mantle cell lymphoma independent of established risk factors. Br J Haematol. 2021;193(3):520-531.
37. Baran-Marszak F, Boukhiar M, Harel S, et al. Constitutive and B-cell receptor-induced activation of STAT3 are important signaling pathways targeted by bortezomib in leukemic mantle cell lymphoma. Haematologica. 2010;95(11):1865.
38. Karvonen H, Chiron D, Niininen W, et al. Crosstalk between ROR1 and BCR pathways defines novel treatment strategies in mantle cell lymphoma. Blood Adv. 2017;1(24):2257-2268.
39. Yang S, Li J-Y, Xu W. Role of BAFF/BAFF-R axis in B-cell non-Hodgkin lymphoma. Crit Rev Oncol Hematol. 2014;91(2):113-122.
40. Zhang L, Yang J, Qian J, et al. Role of the microenvironment in mantle cell lymphoma: IL-6 is an important survival factor for the tumor cells. Blood. 2012;120(18):3783-3792.
41. Novak AJ, Grote DM, Stenson M, et al. Expression of BLyS and its receptors in B-cell non-Hodgkin lymphoma: correlation with disease activity and patient outcome. Blood. 2004;104(8):2247-2253.
42. Medina DJ, Goodell L, Glod J, Gélinas C, Rabson AB, Strair RK. Mesenchymal stromal cells protect mantle cell lymphoma cells from spontaneous and drug-induced apoptosis through secretion of B-cell activating factor and activation of the canonical and non-canonical nuclear factor κB pathways. Haematologica. 2012;97(8):1255-1263.
43. McWilliams EM, Lucas CR, Chen T, et al. Anti–BAFF-R antibody VAY-736 demonstrates promising preclinical activity in CLL and enhances effectiveness of ibrutinib. Blood Adv. 2019;3(3):447-460.

44. Tandler C, Schmidt M, Heitmann JS, et al. Neutralization of B-Cell Activating Factor (BAFF) by Belimumab Reinforces Small Molecule Inhibitor Treatment in Chronic Lymphocytic Leukemia. Cancers. 2020;12(10):2725.
45. Hill HA, Qi X, Jain P, et al. Genetic mutations and features of mantle cell lymphoma: a systematic review and meta-analysis. Blood Adv. 2020;4(13):2927-2938.
46. Hatada EN, Do RK, Orlofsky A, et al. NF-κB1 p50 is required for BLyS attenuation of apoptosis but dispensable for processing of NF-κB2 p100 to p52 in quiescent mature B cells. J Immunol. 2003;171(2):761-768.
47. Paiva C, Rowland TA, Sreekantham B, et al. SYK inhibition thwarts the BAFF-B-cell receptor crosstalk and thereby antagonizes Mcl-1 in chronic lymphocytic leukemia. Haematologica. 2017;102(11):1890.
48. Mondragón L, Mhaidly R, De Donatis GM, et al. GAPDH Overexpression in the T Cell Lineage Promotes Angioimmunoblastic T Cell Lymphoma through an NF-κB-Dependent Mechanism. Cancer Cell. 2019;36(3):268-287.
49. Kennedy R, Klein U. Aberrant activation of NF-κB signalling in aggressive lymphoid malignancies. Cells. 2018;7(11):189.
50. Eluard B, Nuan-Aliman S, Faumont N, et al. The alternative RelB NF-κB subunit is a novel critical player in diffuse large B-cell lymphoma. Blood. 2022;139(3):384-398.

Figure Legends

Figure 1. Microenvironment-dependent and tumor-specific IL32 expression in MCL

(A) Volcano-plot representation of whole transcriptome analysis (publicly available Affimetrix U133, see Methods) from MCL lymph nodes samples (LN, n=107) compared to MCL peripheral blood samples (PB, n=77). Dotted lines indicate the cut-off for significance (padj<0.05, log2Fc >0.5 or < -0.5). The most deeply modulated genes (log2Fc >5 or < -5) are annotated on the graph. **(B)** The diagram represents the comparison of the gene set induced in $CD19^{+}$-sorted PB MCL cultured on CD40L *ex vivo* (RNA-seq, see Methods) with the gene set differentially expressed between MCL LN and PB (panel A). Common *in vivo* and *ex vivo* upregulation (n=3217 genes) were compared to the genes induced in normal CD5+ B cells (NBC) cultured similarly in order to determine “Shared with NBC” and “Tumor-specific” gene sets. **(C)** The graphs represent the top 15 genes of “Shared with NBC” and “Tumor-specific” gene sets, respectively. The score (log2Fc) integrates both *ex vivo* and *in vivo* modulations (log2FC(*ex vivo*)+log2FC(i*n vivo*)). **(D)** IL32 expression was determined at the RNA (RT-qPCR, upper panel) and protein levels (Immunoblot, lower panel) in MCL cell lines.

Figure 2. IL32 is expressed in MCL LN and induced in vitro upon CD40 triggering

(A) *IL32* gene expression in Normal B Cells (NBC, n=24) and MCL cells from Peripheral Blood (PB, n=81) or Lymph Nodes (LN, n=165) was assessed by Gene Expression Profiling (GEP). Mann-Whitney test. ***p < 0.0005, ****p < 0.0001. **(B)** IL32 expression was analyzed by Gene Expression Profiling in paired MCL cells from PB (n=8) or LN (n=8) and by

immunoblot in paired PB and LN tissues (frozen sections) from MCL patients (n=3). *represents higher exposure for immunoblotting. Wilcoxon-matched pairs sign-rank test. **p < 0.008 **(C)** RT-qPCR analysis of *IL32* gene was performed in CD5+ NBC (n=3) or MCL cells (n=13) cultured on CD40L-expressing cells for 7 days. Wilcoxon-matched pairs sign-rank test. ***p<.0005. **(D)** Immunoblot analysis of IL32 protein expression was performed in CD5+ NBC (n=1) or MCL cells (n=4) cultured on CD40L-expressing cells for 7 days.

Figure 3. Protein expression of IL32 in MCL lymph nodes *in situ*. (A) Expression of IL32 was performed using IHC of 1 spleen (SPL) and 3 lymph nodes (LN) sections from 4 MCL patients. Scale bars, 50 µm. **(B,C)** Multiplex Immunohistochemistry staining of Cyclin D1 (opal 570 ; white), CD3 (opal 690 ; green), CD68 (opal 520 ; magenta) and IL32 (opal 650 ; red) was performed on lymph nodes sections from 2 MCL patients (MCL_LN#2, MCL_LN#3). Individual stainings and Dapi are shown in supplementary Figure S9. For MCL-LN#2, the left panel represents a mosaic, the middle panel (Region of interest, ROI#1) a zoom on the sample (Scale bars, 50 µm) and the right panel (ROI#2) represents a projection of 26 Z stacks (range 10 µm; Scale bar 10 µm). For MCL-LN#3, the left panel represents a large area (Scale bar, 100 µm), the middle panel (ROI#1) shows a CD3 infiltrated area and the right panel (ROI#2) represents a tumor-only area (Scale bars, 50 µm).

Figure 4. CD40L-dependent IL32 expression depends on alternative NFκB signaling pathway. (A) Immunoblotting of classical (pIkB) and alternative (p52) NF-kB pathways and IL32 protein was performed in MCL cell lines cultured on CD40L-expressing cells for the indicated time. **(B-C)** RT-qPCR analysis of *IL32* gene **(B)** and immunoblotting of indicated proteins **(C)** were performed in MCL cell lines cultured on CD40L-expressing cells during 96h in the presence or absence of the NIK inhibitor SMI-1 (NIK-i, 10 µM). **(D-E)** Immunoblotting of p52 and IL32 proteins in **(D)** CD19+CD5+ NBC (n=2) or CD19+CD5+ MCL cells (n=3) at D0 and after culture on CD40L-expressing cells for 7 days and **(E)** MCL cell lines (n=10).

Figure 5. Myeloid cells, but not MCL cells, respond to IL32β. (A) Survival of MCL cells (n=8) cultured with or without recombinant human (rh)IL32β (100 ng/ml) for 7 days was measured by lack of Annexin-V staining. Wilcoxon-matched pairs sign-rank test. n.s: not significant. **(B-C)** Immunoblotting of indicated proteins was performed in **(B)** MCL cell lines cultured with or without (rh)IL32β for 6h or **(C)** CD14+ monocytes and CD3+ T cells isolated from healthy donors and cultured with 100 ng/ml of (rh)IL32β for indicated times. **(D)** The figure represents the PCA analysis of monocytes (Mono, n=3), macrophages (Mϕ, n=3) and T-cells (T, n=3) cultured 24h with or without 100 ng/ml of (rh)IL32β. Mϕ were first polarized with M-CSF (50 ng/mL, 5 days) and then stimulated during 48h with 100 ng/ml of (rh)IL32β. Colored ellipses are drawn around the mean of the group (barycenter), with the 95% confidence interval of the mean in the corresponding plan. **(E)** An ascendant hierarchical clustering based on 19203 genes was constructed with ward.D2 method of Euclidian distance.

Figure 6. IL32β secreted by MCL cells induces differentiation of monocytes into protumoral Mϕ-32 macrophages. (A) The figure represents the heat-maps of soluble factor transcripts modulated (log2Fc>0.1) in Monocytes (Mono, n=3) and Monocytes-derived macrophages (Mϕ, n=3) cultured with or without (rh)IL32β as described in Figure 5D. For each cell type, the median gene expression was calculated on normalized and transformed data (DESeq2 package). The colors indicate the intensity of the median gene expression as indicated (log scale). * indicates that gene expression was confirmed by RT-qPCR as represented in Figure S6A. **(B)** The left panel details the experimental protocol related to the right panel. The right panel represents RT-qPCR analysis of 7 genes (*IL1A, IL1B, IL6, IL24, CXCL8, IL32 and BAFF*) in monocytes (Mono) or Monocytes-derived macrophages (Mϕ) cultured, during 24h or 48h respectively, with wild type (-) or IL32$^{-/-}$ (Cr#1) MINO supernatant. **(C)** Forty-eight IL32β-induced soluble factors on Mono or Mϕ were classified as M1-like, M2-

like (upper panel) or MϕMCL-like (lower panel) as previously reported[12]. **(D)** CD163 mean fluorescence intensity ratio was determined by flow-cytometry for M1 (n=3), M2-10 (n=4) and M□-32 (monocytes-derived macrophages differentiated with 50 ng/mL CSF1 during 5 days and then stimulated with 100 ng/mL (rh)IL32β for 48h, n=3) and M□MCL (monocytes-derived macrophages in the presence of MCL cells, n=3). M1, M2-10 and M□MCL were generated as previously described[12]. **(E)** The percentage of MCL live cells was assessed by lack of Annexin-V staining after 3 days of culture alone (-) or with Mϕ32 and separated by transwell inserts (n=10). Wilcoxon-matched pairs sign-rank test. **p < .005.

Figure 7. BAFF supports Mϕ-32 prosurvival effect through activation of alternative NFκB pathway. (A) Schematic representation of the protocol used. **(B)** MCL cells (5.10^5 cells/ml) were cultured with macrophages polarized with IL32 supernatant (s_Mϕ-32, n=6) or growth factors: BAFF (100 ng/mL), IL6 (20 ng/mL), IL10 (100 ng/mL), IL32β (100 ng/mL), TNFa (20ng/mL), IL15 (20 ng/mL), April (100 ng/mL), IL1b (50 ng/mL), IL1a (50 ng/mL), IL24 (100 ng/mL), IL18 (50 ng/mL) or Wnt5a (200 ng/mL) (n≥3). The percentage of cell rescue was assessed after 7 days of *ex vivo* culture. **(C)** Concentration of BAFF protein was evaluated by ELISA in the supernatant of MCL cell lines (n=5), M1 (n=3) and Mϕ-32 (n=5) monocytes-derived macrophages**.** Unpaired t test. *p < 0.05. **(D)** The percentage of cell rescue dependent on Mϕ-32 supernatant (s_Mϕ-32) in MCL cells (n=6) cultured with or without NIK inhibitor (NIK-i, 10 µM) for 7 days was determined by Annexin V staining. Paired t test. *p < 0.05. **(E)** Percentage of cell rescue dependent on Mϕ-32 supernatant (s_Mϕ-32) in primary MCL (n=3) cultured with or without NIK inhibitor (NIK-i, 10 µM) or anti-BAFFR neutralizing antibody (4 µg/mL) for 7 days. (**F)** Immunoblotting of classical (pIkB, IkB) and alternative (p100, p52) NF-kB pathways in MCL cells cultured with Mϕ-32 supernatant (s_Mϕ-32) for 24h with of without anti-BAFFR neutralizing antibody (4 µg/mL) as indicated.

Figure 8. The IL32/BAFF axis supports prosurvival dialogs in the lymphoma ecosystem and is disrupted by NIK inhibition.

Interactions between tumor cells and T cells, through the CD40-CD40L axis, result in activation of NFκB pathways (NFκB1/2) and in NFκB2-dependent secretion of IL32 by tumor cells within their ecosystem. IL32 promoter is hypomethylated in MCL cells compared to normal B cells (NBC) resulting in a tumor-restricted IL32 expression. The latter is involved in monocyte differentiation into lymphoma-associated $CD163^{+}$ macrophages (Mϕ-32). Mϕ-32 are characterized by a specific secretome, which includes BAFF, and support a BAFFR/ NFκB2-dependent tumoral survival. Selective NIK inhibition counteracts NFκB2 activation and consequently prevents both IL32 secretion by MCL cells and BAFF-dependent MCL-survival.

Figure 1

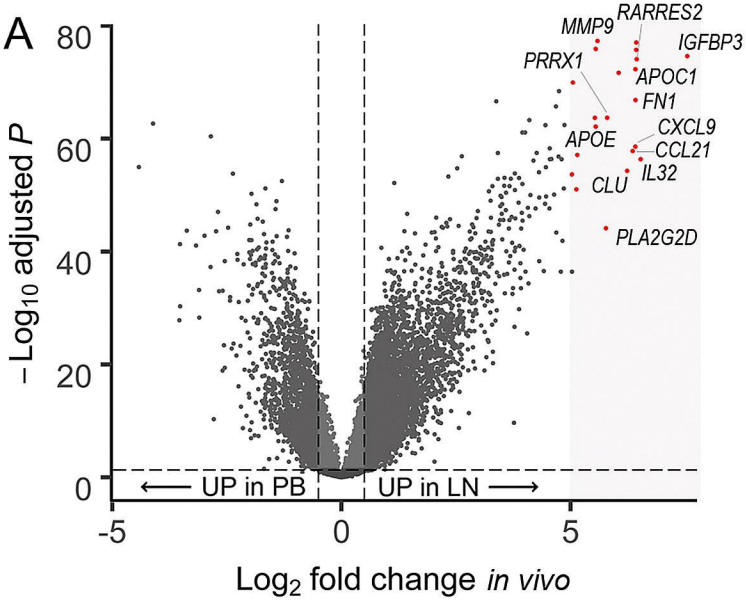
A
80
60
40
20
0
– Log10 adjusted P
MMP9
RARRES2
IGFBP3
PRRX1
APOC1
FN1
CXCL9
APOE
CCL21
IL32
CLU
PLA2G2D
⟵ UP in PB
UP in LN ⟶
-5
0
5
Log2 fold change in vivo

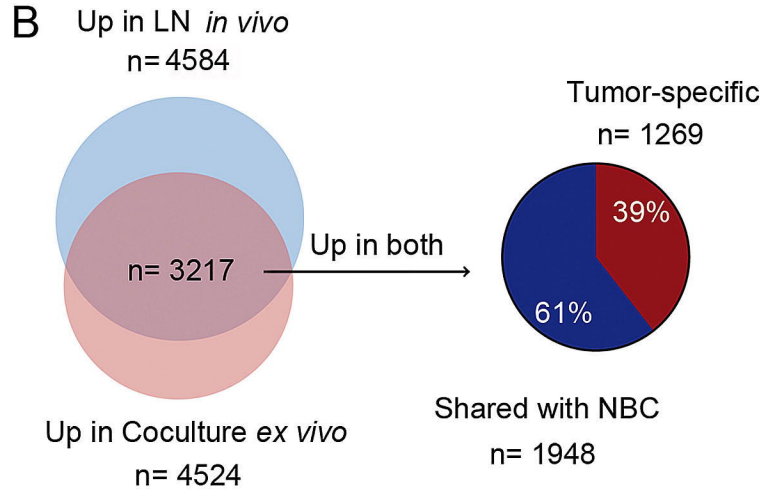
B
Up in LN in vivo
n= 4584
n= 3217
Up in Coculture ex vivo
n= 4524
Up in both
Tumor-specific
n= 1269
39%
61%
Shared with NBC
n= 1948

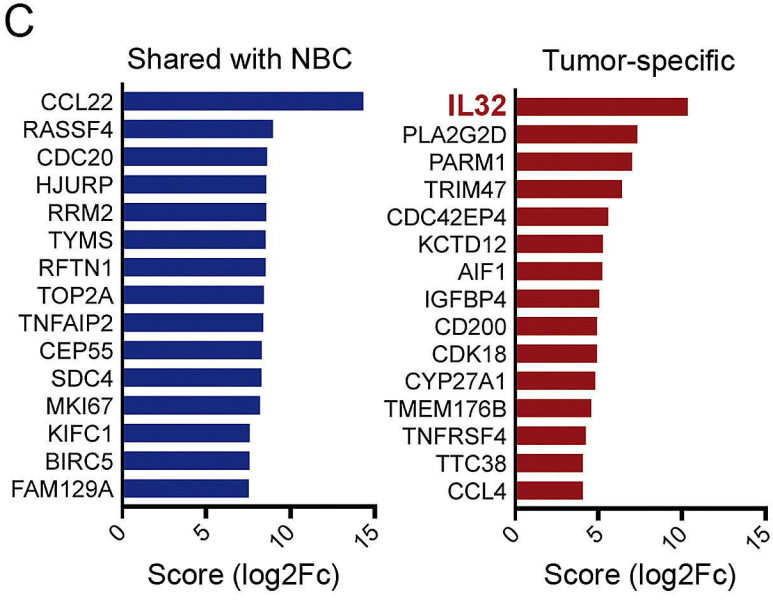
C
Shared with NBC
CCL22
RASSF4
CDC20
HJURP
RRM2
TYMS
RFTN1
TOP2A
TNFAIP2
CEP55
SDC4
MKI67
KIFC1
BIRC5
FAM129A
0
5
10
15
Score (log2Fc)
Tumor-specific
IL32
PLA2G2D
PARM1
TRIM47
CDC42EP4
KCTD12
AIF1
IGFBP4
CD200
CDK18
CYP27A1
TMEM176B
TNFRSF4
TTC38
CCL4
0
5
10
15
Score (log2Fc)

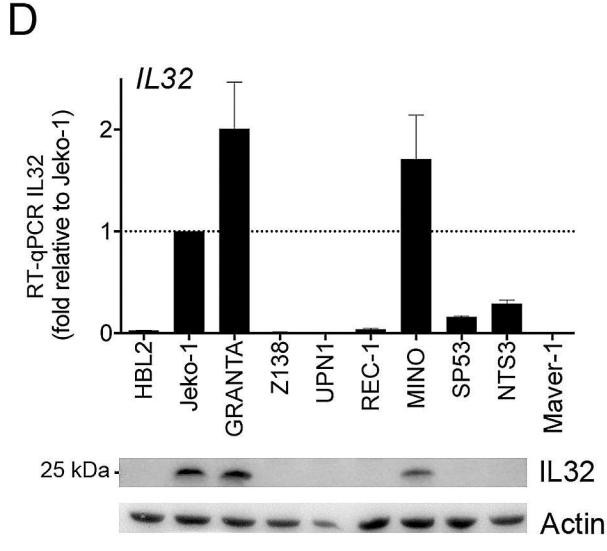
D
IL32
RT-qPCR IL32
(fold relative to Jeko-1)
2
1
0
HBL2
Jeko-1
GRANTA
Z138
UPN1
REC-1
MINO
SP53
NTS3
Maver-1
25 kDa
IL32
Actin

Figure 2

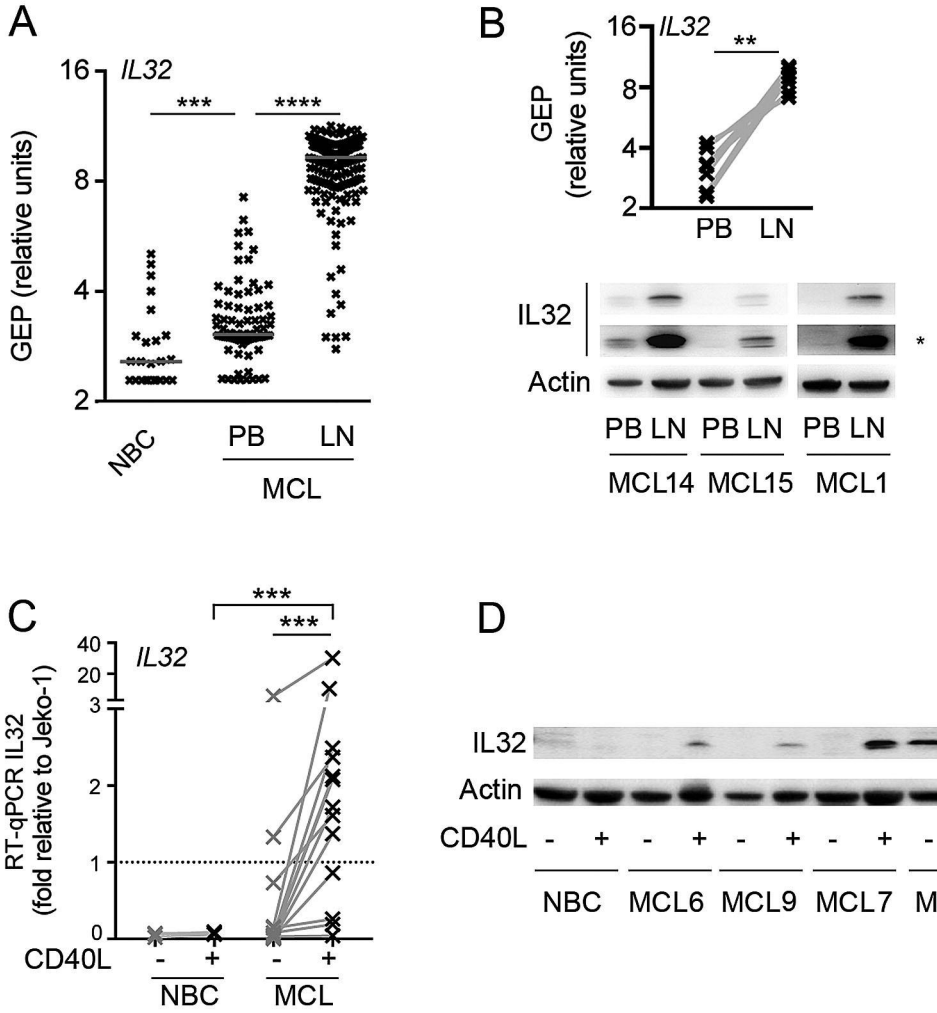
A
IL32
GEP (relative units)
16
8
4
2
***
****
NBC
PB
LN
MCL
B
IL32
GEP (relative units)
16
8
4
2
**
PB
LN
IL32
Actin
*
PB LN PB LN PB LN
MCL14 MCL15 MCL1
C
IL32
RT-qPCR IL32 (fold relative to Jeko-1)
40
20
3
2
1
0
***
***
CD40L - + - +
NBC
MCL
D
IL32
Actin
CD40L - + - + - + - + - +
NBC MCL6 MCL9 MCL7 MCL5

Figure 3

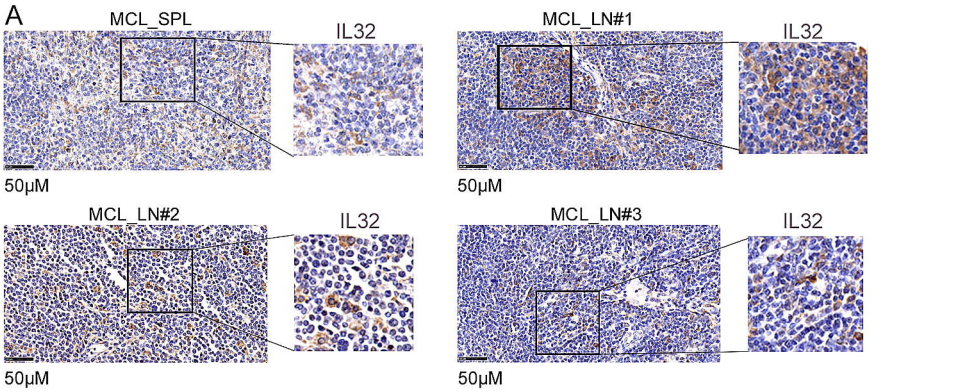
A
MCL_SPL
IL32
50μM
MCL_LN#1
IL32
50μM
MCL_LN#2
IL32
50μM
MCL_LN#3
IL32
50μM

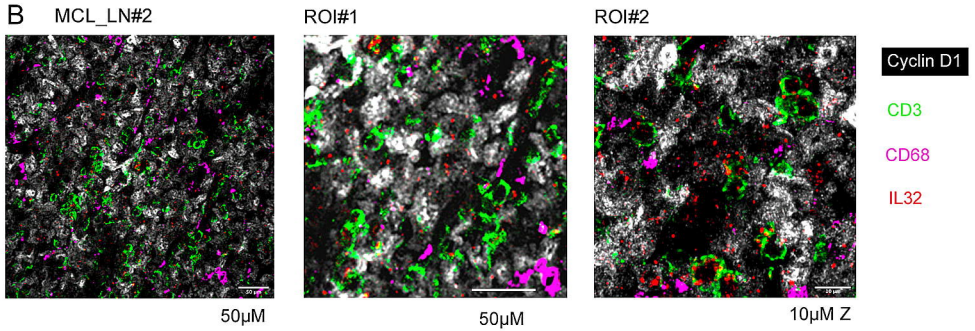
B
MCL_LN#2
ROI#1
ROI#2
Cyclin D1
CD3
CD68
IL32
50μM
50μM
10μM Z

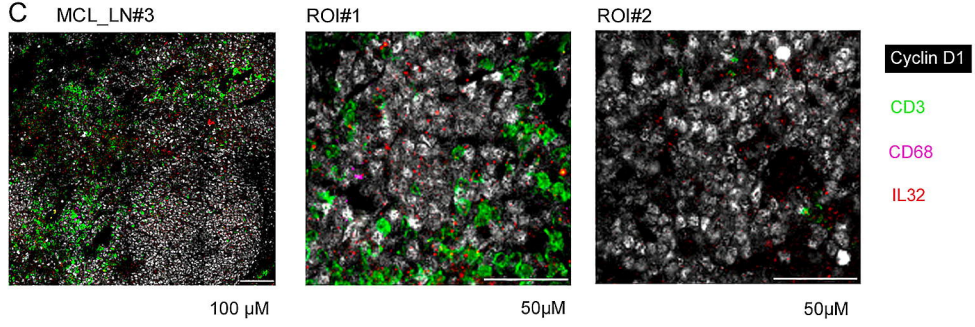
C
MCL_LN#3
ROI#1
ROI#2
Cyclin D1
CD3
CD68
IL32
100 μM
50μM
50μM

Figure 4

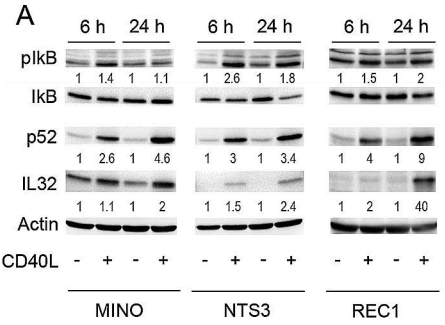
A
6 h
24 h
6 h
24 h
6 h
24 h
pIkB
1 1.4 1 1.1
1 2.6 1 1.8
1 1.5 1 2
IkB
p52
1 2.6 1 4.6
1 3 1 3.4
1 4 1 9
IL32
1 1.1 1 2
1 1.5 1 2.4
1 2 1 40
Actin
CD40L - + - + - + - + - + - +
MINO
NTS3
REC1

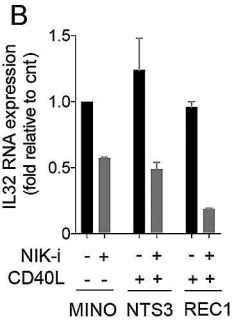
B
IL32 RNA expression (fold relative to cnt)
1.5
1.0
0.5
0
NIK-i - + - + - +
CD40L - - + + + +
MINO
NTS3
REC1

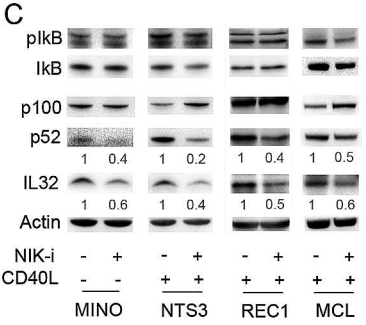
C
pIkB
IkB
p100
p52
1 0.4 1 0.2 1 0.4 1 0.5
IL32
1 0.6 1 0.4 1 0.5 1 0.6
Actin
NIK-i - + - + - + - +
CD40L - - + + + + + +
MINO
NTS3
REC1
MCL

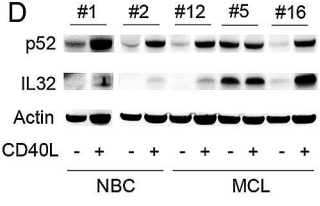
D
#1
#2
#12
#5
#16
p52
IL32
Actin
CD40L - + - + - + - + - +
NBC
MCL

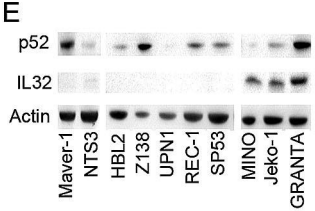
E
p52
IL32
Actin
Maver-1
NTS3
HBL2
Z138
UPN1
REC-1
SP53
MINO
Jeko-1
GRANTA

Figure 5

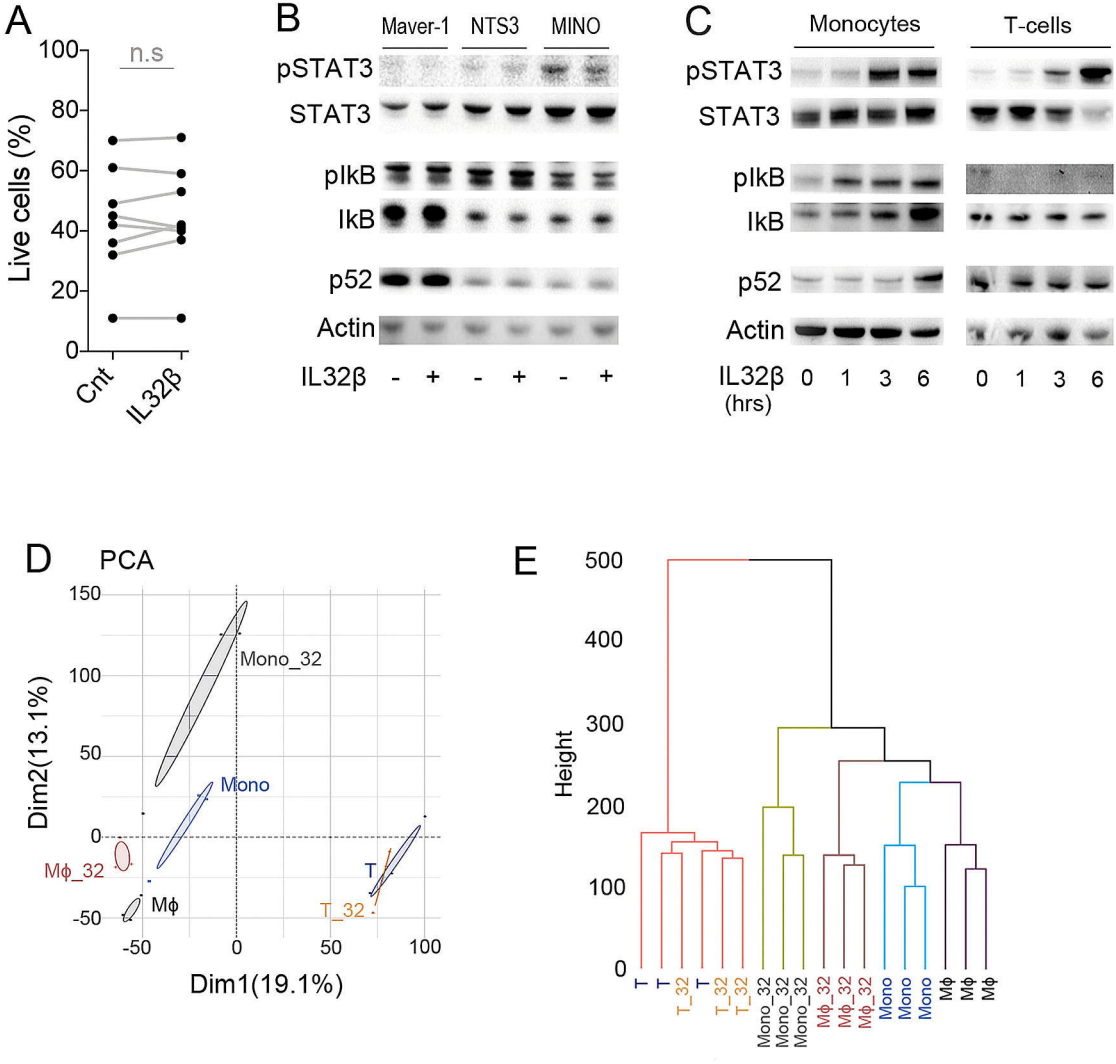
A
n.s
Live cells (%)
100
80
60
40
20
0
Cnt
IL32β
B
Maver-1
NTS3
MINO
pSTAT3
STAT3
pIkB
IkB
p52
Actin
IL32β - + - + - +
C
Monocytes
T-cells
pSTAT3
STAT3
pIkB
IkB
p52
Actin
IL32β (hrs) 0 1 3 6 0 1 3 6
D
PCA
Dim2(13.1%)
Dim1(19.1%)
Mono_32
Mono
Mϕ_32
Mϕ
T
T_32
E
Height
500
400
300
200
100
0
T
T
T_32
T
T_32
T_32
Mono_32
Mono_32
Mono_32
Mϕ_32
Mϕ_32
Mϕ_32
Mono
Mono
Mono
Mϕ
Mϕ
Mϕ

Figure 6

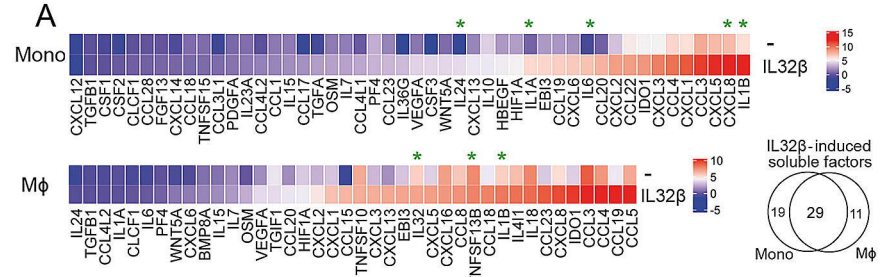
A
Mono
Mϕ
IL32β
IL32β-induced soluble factors
19
29
11
Mono
Mϕ

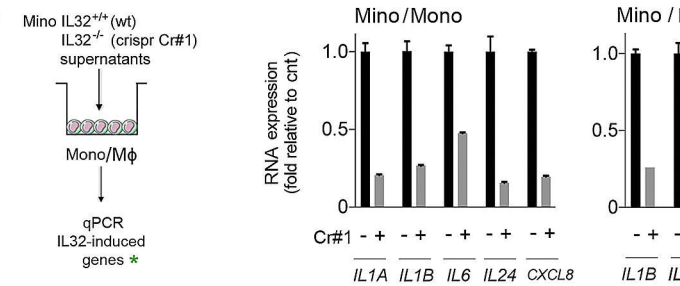
B
Mino IL32+/+ (wt)
IL32-/- (crispr Cr#1)
supernatants
Mono/Mϕ
qPCR
IL32-induced genes *
Mino/Mono
Mino / Mϕ
RNA expression (fold relative to cnt)
Cr#1
IL1A
IL1B
IL6
IL24
CXCL8
IL1B
IL32
BAFF

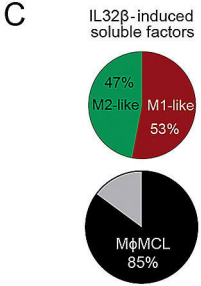
C
IL32β-induced soluble factors
47%
M2-like
M1-like
53%
MϕMCL
85%

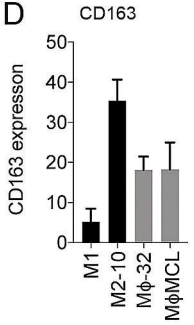
D
CD163
CD163 expresson
M1
M2-10
Mϕ-32
MϕMCL

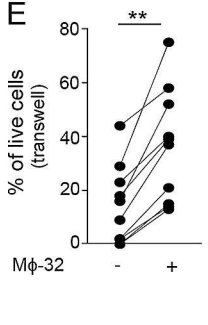
E
**
% of live cells (transwell)
Mϕ-32

Figure 7

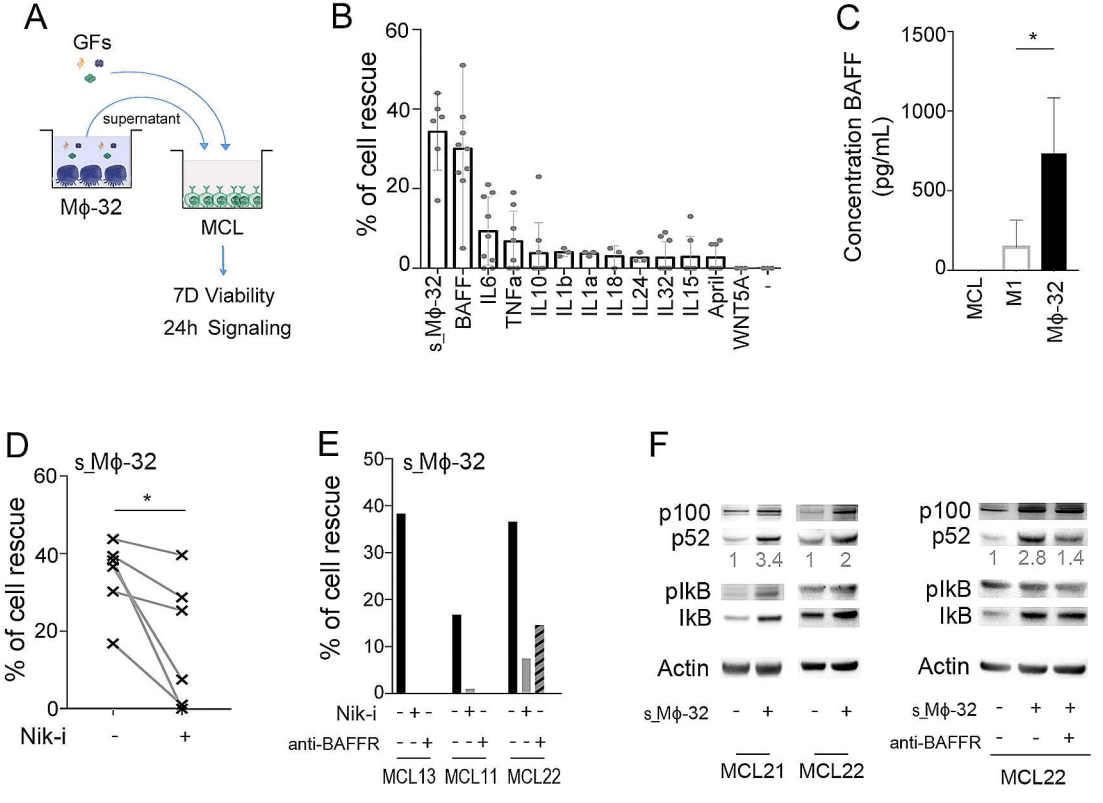
A
GFs
supernatant
Mϕ-32
MCL
7D Viability
24h Signaling
B
% of cell rescue
60
40
20
0
s_Mϕ-32
BAFF
IL6
TNFa
IL10
IL1b
IL1a
IL18
IL24
IL32
IL15
April
WNT5A
C
Concentration BAFF (pg/mL)
1500
1000
500
0
*
MCL
M1
Mϕ-32
D
s_Mϕ-32
% of cell rescue
60
40
20
0
*
Nik-i
-
+
E
s_Mϕ-32
% of cell rescue
50
40
30
20
10
0
Nik-i - + - - + - - + -
anti-BAFFR - - + - - + - - +
MCL13 MCL11 MCL22
F
p100
p52
1 3.4 1 2
pIkB
IkB
Actin
s_Mϕ-32 - + - +
MCL21 MCL22
p100
p52
1 2.8 1.4
pIkB
IkB
Actin
s_Mϕ-32 - + +
anti-BAFFR - - +
MCL22

Figure 8

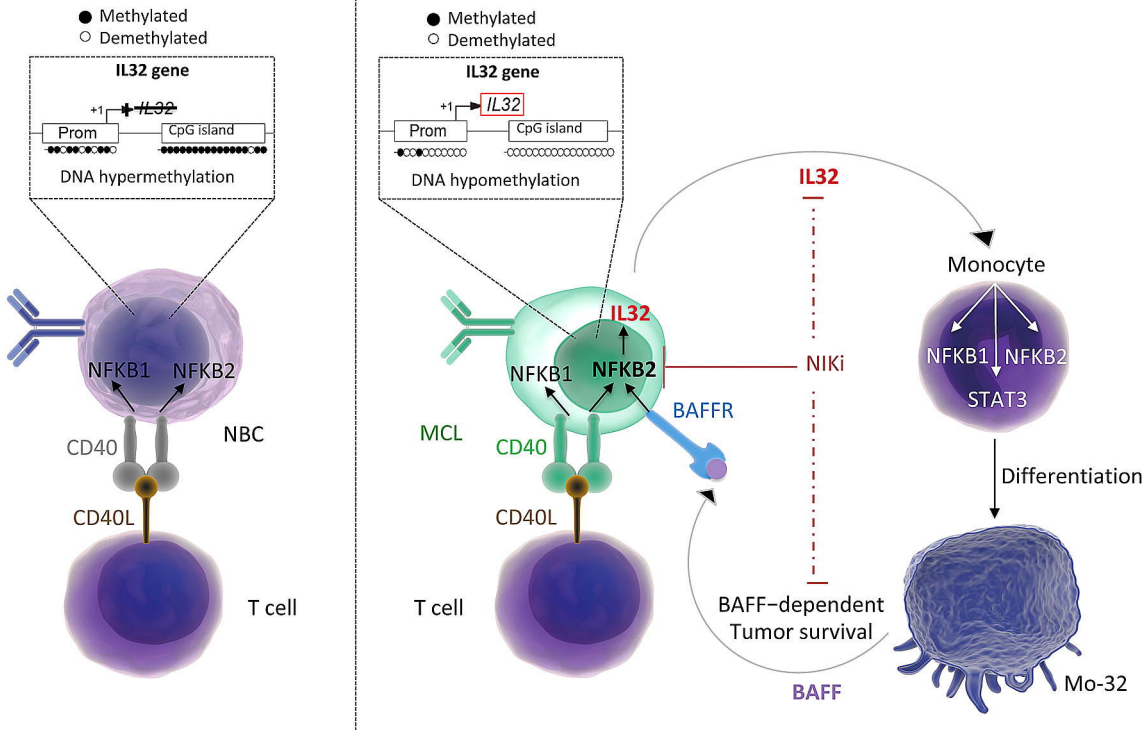
Methylated
Demethylated
IL32 gene
+1
IL32
Prom
CpG island
DNA hypermethylation
NFKB1
NFKB2
NBC
CD40
CD40L
T cell
Methylated
Demethylated
IL32 gene
+1
IL32
Prom
CpG island
DNA hypomethylation
IL32
NFKB1
NFKB2
NIKi
BAFFR
MCL
CD40
CD40L
T cell
IL32
Monocyte
NFKB1
NFKB2
STAT3
Differentiation
BAFF−dependent
Tumor survival
BAFF
Mo-32

Supplemental Files

The IL32/BAFF axis supports prosurvival dialogs in the lymphoma ecosystem and is disrupted by NIK inhibition

Decombis et al.

Supplemental information includes supplemental Methods, 3 supplemental tables, 9 supplemental figures and legends and supplemental references

Supplemental Methods

MCL cell lines

JeKo-1, MINO, REC-1, MAVER-1, and GRANTA-519 were purchased from DSMZ (Braunschweig, Germany) and Z138 from ATCC (Manassas, USA). UPN1, HBL2 and SP53 were kindly provided by Prof. V. Ribrag (Institut Gustave Roussy Villejuif, France), Prof. M Callanan (INSERM, CHU de Dijon, France) and Prof. S. Chen-Kiang (Cornell University, NY), respectively. NTS3 cell line has been generated in our laboratory (characterized by GEP, GSE86322). Cell lines are routinely identified using a flow cytometry-based barcode as well as MHC class I sequencing[1].

Genome editing using the CRISPR-Cas9 system

To generate IL32$^{-/-}$ MCL cells, we infected MINO and NTS3 cells with lentiviruses encoding for Cas9-mcherry (Addgene plasmid # 70182), and mCherry positive cells were sorted using FACSAria Cell sorter (Cytocell, SFR Bonamy, Nantes). Sorted cells were then infected with lentiviruses containing *GFP* and doxycycline-inducible sgRNA (Addgene plasmid # 70183) directed against IL32. The designed crRNA targeted the following sequence in *IL32* gene: 5'-GGCCGCCATGTGCTTCCCGA-3'. GFP positive cells were sorted and sgRNA expression was induced. Cells were cloned by limiting dilutions from the bulk prior characterization of IL32 knockout by DNA sequencing and protein analysis (Figure S7).

Secretome quantification

Monocytes were differentiated with CSF1 (50 ng/mL) with or without (rh)IL32β (100 ng/ml) during 3 days, supernatant was collected and soluble factors were quantified by cytokine array (Proteome Profiler Human Cytokine Array Kit, R&D Systems). Pixel densities were analyzed by using the Image Lab Software (Bio-Rad). Regarding IL32, concentration was determined in MCL cell line supernatants using Human IL32 duoset Elisa (R&D systems). BAFF concentration was determined using Human BAFF / TNFSF13B Elisa kit PicoKine^{TM} (Boster).

Bioinformatics analysis

Gene Expression Profiling (GEP)

.CEL files were downloaded and processed in R-3.6.1 using the affy package, optical noise/background correction was performed by gcrma with standard options, and expression batches were finally normalized by quantiles using the limma package. Differential gene expression was assessed with limma package (up regulated gene: log2Fc>0.5; adjusted

p<0.05) and we used the GAGE package (KEGG pathway analysis) for gene set enrichment analysis.

Full-length RNA-seq:

Total RNA was extracted with RNeasy Mini kit (Qiagen) and quantified using a Nanodrop®ND-1000 spectrophotometer (Thermo Scientific). Quality and integrity of RNA samples were assessed using the 2100 Bioanalyzer and RNA 6000 Nano LabChip kit series II (Agilent Technologies). Library construction was performed from 500ng of total RNA with SureSelect Strand-Specific RNA Library Prep for Illumina Multiplexed kit (Ref 5190-6410, Agilent Technologies) according to Agilent_PrepLib_G9691-90010_juillet2015_vD protocol. Purifications were carried out with NucleoMag NGS Clean-up and Size Select (Ref 744970.50, Macherey-Nagel). Fragments size of libraries was controlled on D1000 ScreenTape with 2200 TapeStation system (Agilent Technologies). Libraries with P5-P7 adaptors were specifically quantified on LightCylcer ® 480 Instrument II (Roche Life Science) and normalized with DNA Standards (1-6) (Ref KK4903, KAPABIOSYSTEMS - CliniSciences). Each library was pooled and prepared according to Denaturing and diluting libraries protocol for the Hiseq and GAIIx, part#15050107 v02 (Illumina) for cluster generation on cBotTM system. Paired-end sequencing (2x100 cycles) was carried out with 4 samples by lane on HiSeq® 2500 system (Illumina) in TruSeq v3 chemistry according to the instructions of HiSeq® 2500 System Guide, part#15035786 v01 (Illumina).

After demultiplexing and quality control with fastQC_0.11.2 (http://www.bioinformatics.babraham.ac.uk/projects/fastqc/), illumina adapter were trimmed with cutadapt-1.2.1[2] and reads with Phred quality score below 30 were filtered with prinseq-lite-0.20.3[3]. Reads were aligned against human hg19 reference genome with tophat2.0.10[4], reads count and differential analysis was realized with Gfold[5].

Relative abundance of 9 known transcripts of IL32 was performed with Pennseq[6] using refseq annotation downloaded from UCSC.

3'seq-RNA Profiling

3'seq-RNA Profiling protocol is performed according to Soumillon et al.[7] The mRNA poly(A) tails are tagged with universal adapters, well-specific barcodes and unique molecular identifiers (UMIs) during template-switching reverse transcriptase. Barcoded cDNAs from multiple samples are then pooled, amplified and tagmented using a transposon-fragmentation approach, which enriches for 3′ends of cDNA. A library of 350–800 bp length is run on an Illumina NovaSeq 6000 using NovaSeq 6000 SP Reagent Kit 100 cycles (ref #20027464).

Raw fastq pairs used for analysis matched the following criteria: the 16 bases of the first read correspond to 6 bases for a designed well-specific barcode and 10 bases for a unique molecular identifier (UMI). The second read (58 bases) corresponds to the captured poly(A) RNAs sequence. We perform demultiplexing of these fastq pairs according to the samplesheet to generate one single-end fastq for all samples. These fastq files are then aligned with bwa to the reference mRNA sequences and the mitochondrial genomic sequence, both available from the UCSC download site. DGE profiles are generated by parsing the alignment files (.bam) and counting for each sample the number of unique UMIs associated with each RefSeq genes. Reads aligned on multiple genes, containing more than one mismatch with the reference sequence or reads containing a polyA pattern are discarded. Finally, a matrix containing the expression of all genes on all samples is produced. The expression values, corresponding to the absolute abundance of mRNAs in all samples, is then ready for further gene expression analysis. DESeq2 is used to normalize expression with the DESeq[8]. Normalized counts are transformed with vst (variance stabilized transformation) function from DESeq library. Batch effects may be corrected with the limma library function "removeBatchEffect".

***IL32* locus-specific methylation analysis**

Genomic DNA was extracted with QIAamp DNA Blood Mini kit (Qiagen) and treated with bisulfite (Active-Motif). The converted DNA was amplified by specific nested PCR for promoter and CpG island of *IL32* (Table S3). The cloning step was realized with StrataClone PCR Cloning Kit (Stratagene). Extracted DNA from the selected colonies (Miniprep Plasmid DNA purification, Macherey Nagel) was sequenced and analyzed (n=8 clones per sample).

Immunohistochemistry (IHC)

Classic IHC

Formalin-fixed paraffin-embedded (FFPE) tissue sections of 3 lymph nodes and 1 spleen from 4 MCL patients were obtained from Pathological Anatomy Department, CHU, Nantes, France. For IHC staining, the sections were subjected to pretreatment involving antigen retrieval by heating in EDTA buffer. Samples were then incubated with an anti-IL32 antibody and with the Impath DAB OB Sens Detection kit (A. Menarini Diagnostics, France) for revelation. The experiment was realized in the automated Impath36 (A. Menarini Diagnostics, France). Histopathology slides were scanned with a Nanozoomer 2.0 HT (Hamamatsu Photonics K. K., Japan). Negative controls for IHC were included in each run, and consisted in replacing the primary antibody with Rabbit Primary Antibody Isotype Control (2 µg/mL IgG) (GBI Labs, USA).

Other methods

Viability assays (Annexin-V staining) as well as real-time quantitative reverse transcription polymerase chain reaction (RT-qPCR, control gene RPL37A) and immunoblot protocols have been previously described [9]. Statistical analyses were performed using two-sided Mann–Whitney, Wilcoxon-matched pairs signed-rank, or t-tests as stated in the Figure legends. Analyses were performed using Graph-Pad Prism and R statistical softwares and all tests were considered statistically significant at $p < 0.05$.

Supplemental Tables

MCL#	Age	Status	%CD19+/CD5+	Subtype at D	SOX11	TP53	Constitutive IL32
1	74	D	57	LNN	-	wt	-
2	22	R	75	Conventional	+	wt	-
2_PE	69	R	75	Conventional	+	wt	+
3	73	D	80	Conventional	+	wt	-
4	66	D	80	Conventional	+	wt	+
5	73	R	67	Blastoid	+	abn	+
6	65	D	43	LNN	-	wt	-
7	80	R	77	Conventional	+	wt	-
8	81	R	66	LNN	-	abn	-
9	73	R	70	Conventional	*ND*	wt	*ND*
10	60	D	87	LNN	-	wt	-
11	74	D	87	Conventional	+	wt	-
12	82	D	92	Conventional	+	wt	-
13	78	R	94	LNN	-	wt	-
14	81	R	22	Conventional	+	wt	+
15	75	D	88	Blastoid	+	abn	-
16	71	R	90	Blastoid	+	wt	-
17	80	R	78	Conventional	+	wt	+
18	70	R	79	Conventional	*ND*	abn	*ND*
19	60	R	77	Conventional	+	wt	-
20	60	D	50	Conventional	*ND*	wt	*ND*
21	68	D	60	LNN	-	abn	-
22	57	D	68	Conventional	+	wt	-
23	53	D	35	LNN	-	*ND*	-

Lines	SOX11	TP53	Constitutive IL32
HBL2	+	abn	-
Jeko	+	abn	+
GRANTA	+	wt	+
Z138	+	wt	-
UPN1	+	abn	-
REC1	+	abn	-
MINO	+	abn	+
SP53	+	wt	-
NTS3	+	wt	-
MAVER	+	abn	-

Supplemental Table S1

Patient samples and cell lines information. D, Diagnosis; R, Relapse; LNN, Leukemic Non Nodal. wt: wild type, abn: abnormal.

All samples came from peripheral blood excepted 2_PE form Pleural Effusion

SOX11 and IL32 expression were determined by 3'seq-RNA Profiling of peripheral blood samples. TP53 status was determined by targeted sequencing of *TP53* and/or in vitro response to Nulin3a.

Primary antibodies for Immunoblot			
Specificity	**Clone**	**Source**	**Reference**
Anti Actin	C4	Merck Millipore	MAB1501
Anti GAPDH	G-9	Santa Cruz	sc-365062
Anti IL-32	Polyclonal	Atlas Antibodies	HPA029397
Anti NF-KB p52-p100	Monoclonal	Merck	05-361
Anti NF-KB Anti p50-p105	Polyclonal	Santa cruz	sc-114
Anti Stat 3 (P) Tyr-705	D3A7	Cell signaling	9145
Anti Stat 3	Monoclonal	Biosciences	610190
Anti IκBα (P) Ser 32/34	5A5	Cell signaling	9246S
Anti IκBα	Polyclonal	Cell signaling	9242S
Anti MCL1	22	Santa Cruz	sc-12756
Anti A1	D1A1C	Cell signaling	#14093S
Anti BclxL	D3	Santa Cruz	sc271121

Antibodies and reagents for flow-cytometry		**Clone**	**Source**
Phenotype	anti-CD14-PE	RMO52	Beckman coulter
	anti-CD163-APC	REA812	BD Pharmingen
	Anti-BAFFR-PE	8A7	eBiosciences,
	Anti-BAFFR-PE	11C1	BD Pharmingen
Viability	Annexin V-APC		Beckman coulter

Antibodies and reagents for IHC		**Clone**	**Source**
Antibodies	IL32	Polyclonal	Atlas Antibodies
	Cyclin D1	SP4	Thermo Scientific
	CD3	Polyclonal	Dako
	CD68	PG-M1	Dako
Retrieval solutions	Envision FLEX Target Retrieval solution High pH		Dako
	TR1 Retrieval solution		A. Menarini Diagnostics

TaqMan gene expression assays		**Source**
IL1a	Hs00174092_m1	Applied Biosystems
IL1b	Hs01555410_m1	
IL6	Hs00174131_m1	
IL24	Hs01114274_m1	
IL32	Hs00992441_m1	
BAFF	Hs04234384_m1	
CXCL8	Hs00174103_m1	
RPL37A	Hs01102345_m1	

Reagents and antibodies for treatment		**Source**
Drugs	NIK SMI1	MedChemExpress
	Ibrutinib, BMS-345541	SelleckChem
Neutralizing antibodies	Anti-BAFFR, Anti-BAFF	R&D Systems
Cytokines	IL1a, IL1b, IL10, IFNg, April, BAFF, CSF1, CSF2	Peprotech
	IL6, IL18, IL24, IL32b, TNFa,Wnt5a	R&D Systems
	IGF1	Sigma-Aldrich
	IL15	Serotec

Supplemental Table S2: Antibodies and reagents

Specific nested PCR for CpG island (CPGI): PCR1 F1-R1 and PCR2 F2-R2	
Primer name	Sequence
IL32CPGI-F1	GAGGATTTTTTGGGGAGGAGGGTGT
IL32CPGI-R1	AACACCAAAACCCACACAAACCTTA
IL32CPGI-F2	TGAGATATTTTTTTTTTTTTATATT
IL32CPGI-R2	TACTCTTAAACCCACCCAACTAAAC
Specific nested PCR for promoter: PCR1 F3-R3 and PCR2 F2-R3	
Primer name	Sequence
IL32promoter-F3	AGGTTTAGTTAGGTTGGAGGGTTAG
IL32promoter-R3	CAAACAAAAACAAAAACAAAAACAA
IL32promoter-F2	GGGGAGTTTTAAGATTGTTGAGATT

Supplemental Table S3

IL-32 promoter and CpG island nested PCR primers for methylation analysis

A

Gene_Name	Regulation	log2FC	Top Prediction	score (%)	source
IGFBP3	Up in LN	7.55	Extracellular region	91	PSORT
IL32	Up in LN	6.53	Extracellular region	44	PSORT
COL6A3	Up in LN	6.44	Extracellular region	50	PSORT
PTGDS	Up in LN	6.43	Extracellular region	78	PSORT
RARRES2	Up in LN	6.43	Extracellular region	97	PSORT
FN1	Up in LN	6.42	Extracellular region	53	PSORT
APOC1	Up in LN	6.42	Extracellular region	100	PSORT
CCL21	Up in LN	6.41	Extracellular region	100	Yloc
CXCL9	Up in LN	6.36	Extracellular region	100	Yloc
CLU	Up in LN	6.24	Plasma membrane	47	PSORT
C1S	Up in LN	6.07	Extracellular region	75	PSORT
PRRX1	Up in LN	5.80	Nucleus	100	PSORT
PLA2G2D	Up in LN	5.77	Extracellular region	97	PSORT
MMP9	Up in LN	5.59	Extracellular region	59	PSORT
APOE	Up in LN	5.55	Extracellular region	78	PSORT
VWF	Up in LN	5.54	Extracellular region	81	PSORT
C3	Up in LN	5.53	Extracellular region	91	Yloc
CPE	Up in LN	5.16	Extracellular region	99	Yloc
ADAMDEC1	Up in LN	5.13	Extracellular region	78	PSORT
C10orf10	Up in LN	5.06	Mitochondrion	47	PSORT
LTF	Up in LN	5.03	Extracellular region	75	PSORT
C1QA	Up in LN	5.03	Extracellular region	63	PSORT

B

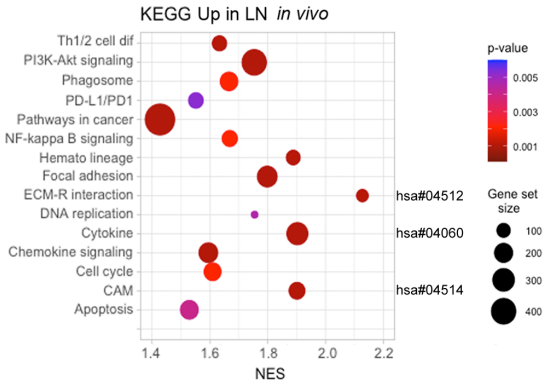

C

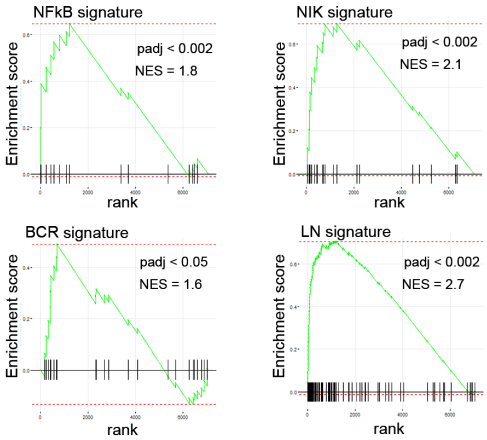

D

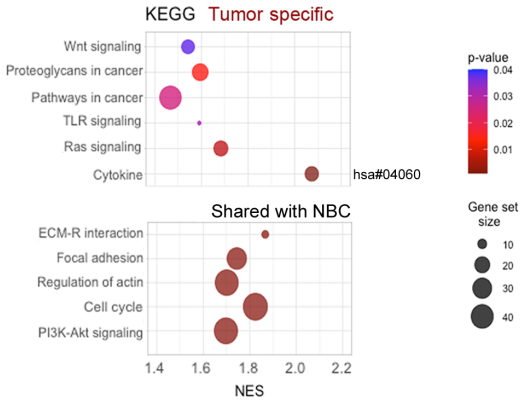

Supp. Fig. S1_Functional annotations and signature enrichment in vivo and ex vivo

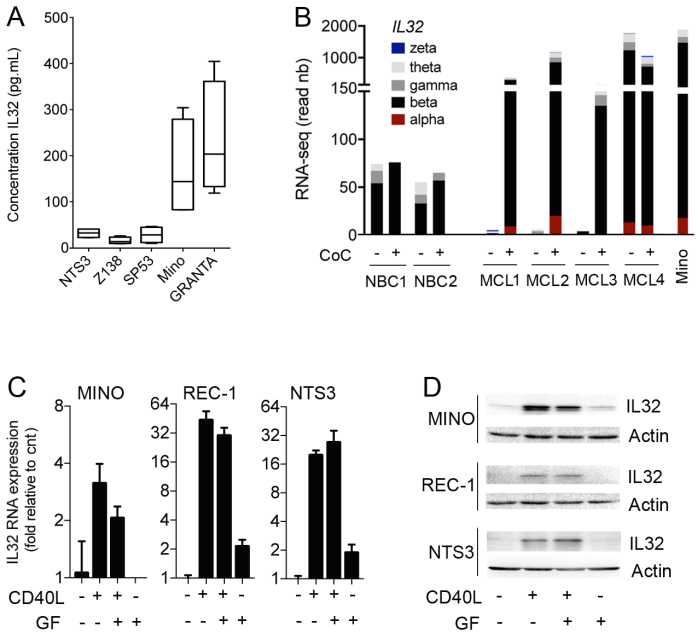

Supp. Fig. S2 _ IL32 is expressed and induced by CD40L in MCL cell lines

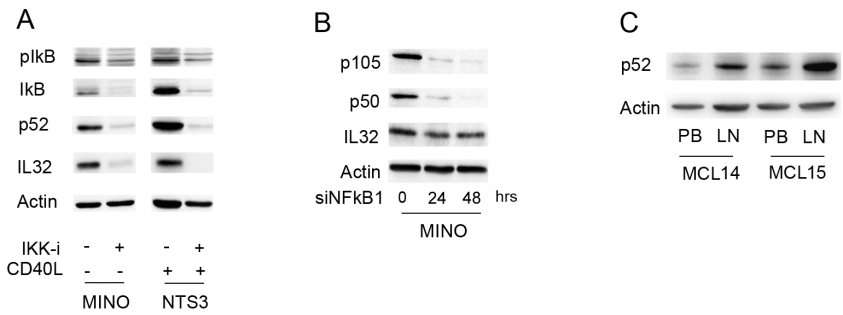

Supp. Fig. S3_ Alternative but not classical NFkB is involved in CD40-induced IL32 expression

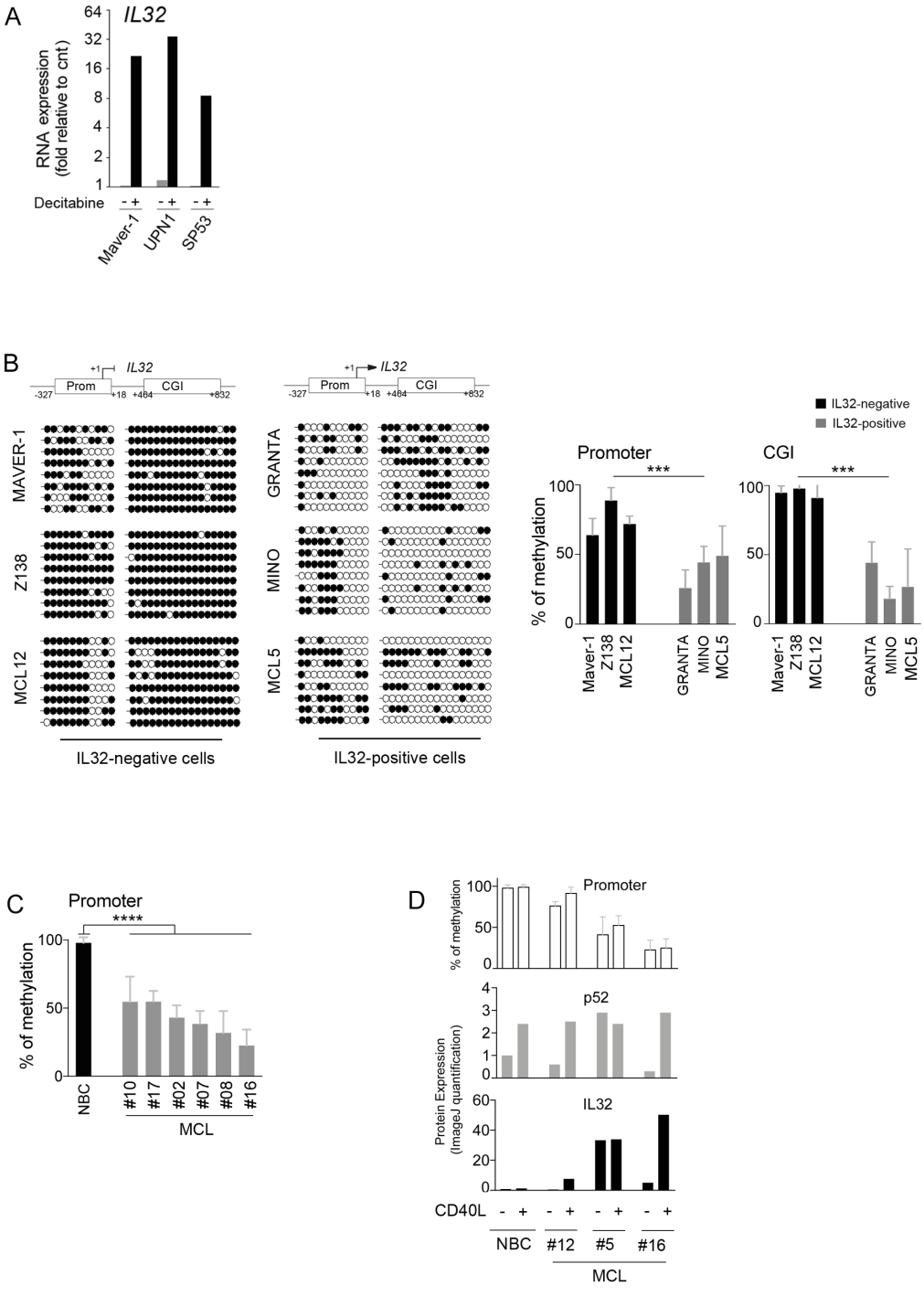

Supp. Fig. S4_Tumor-specific expression of IL32 is due to epigenetic regulations

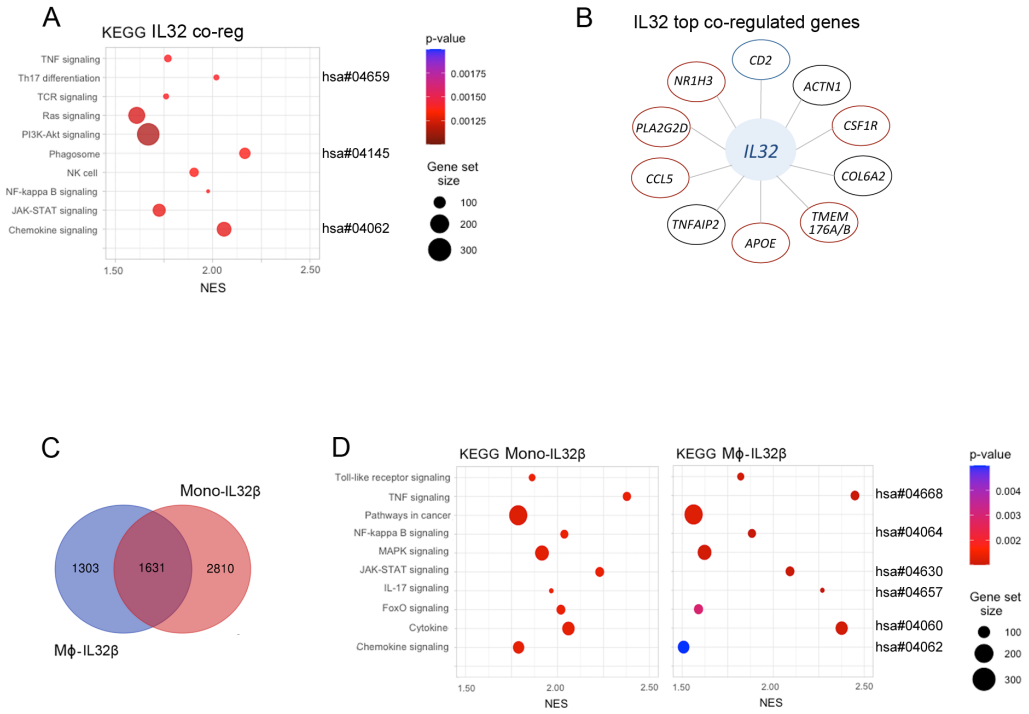

Supp. Fig. S5_IL32 is coregulated with genes expressed by monocytes and T cells in MCL LN

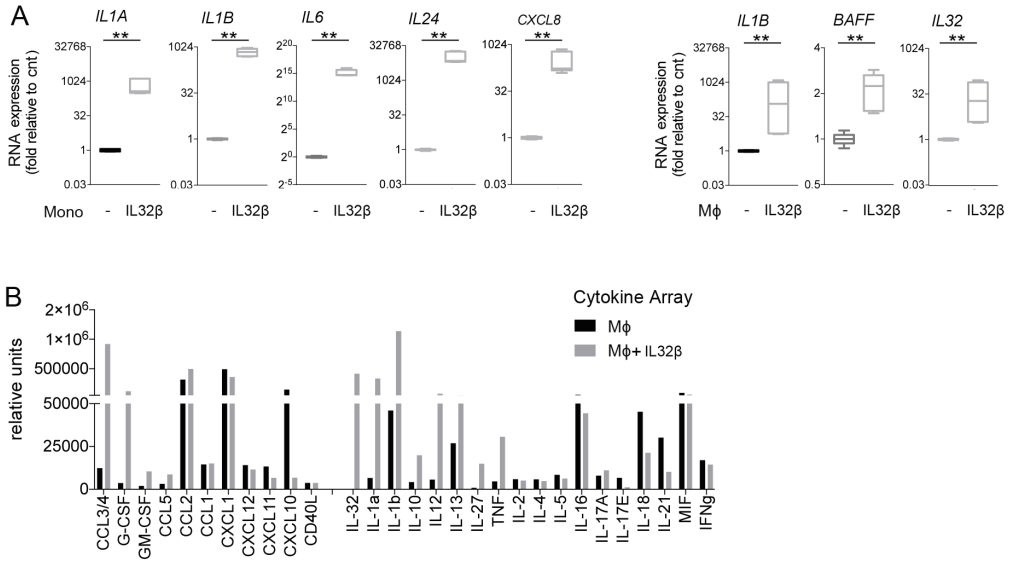

Supp. Fig. S6_ Secretome of IL32-stimulated monocytes and macrophages

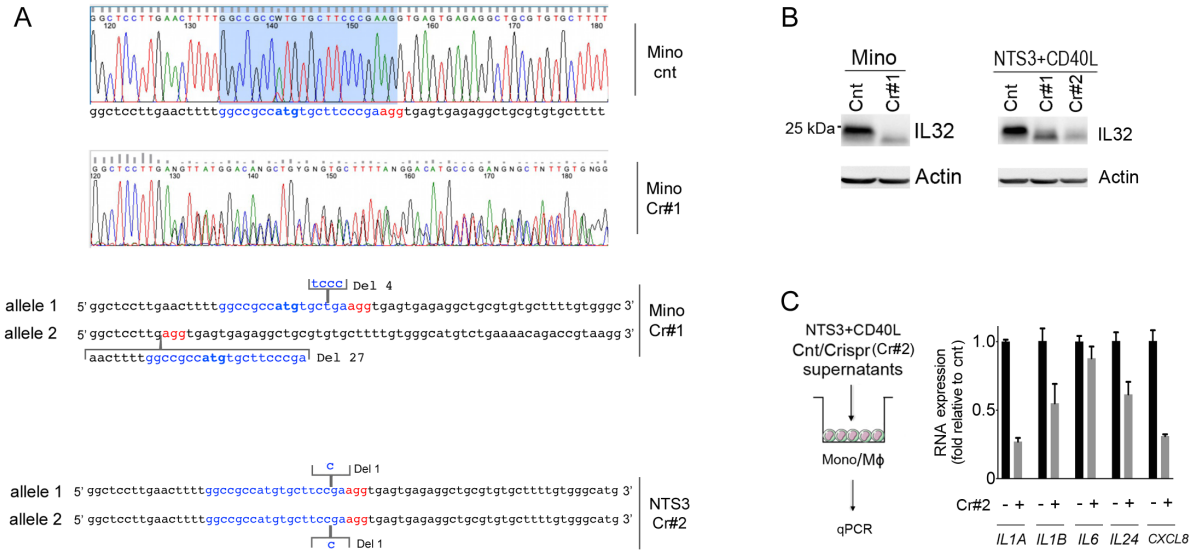

Supp. Fig. S7_ Generation of IL32KO Mino and NTS3 cells through Crisp/Cas9 technology

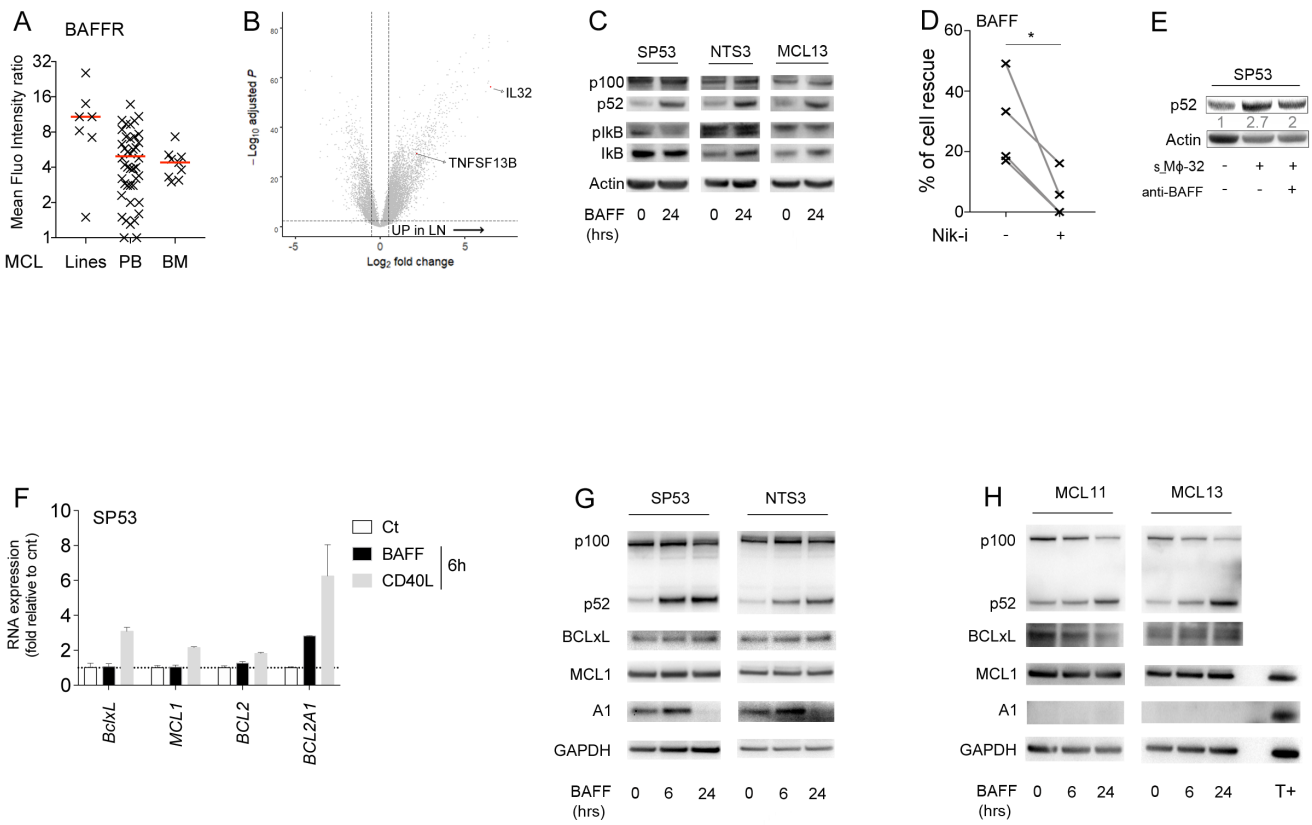

Supp. Fig. S8_ BAFF-specific MCL cell rescue is dependent on alternative NFkB pathway

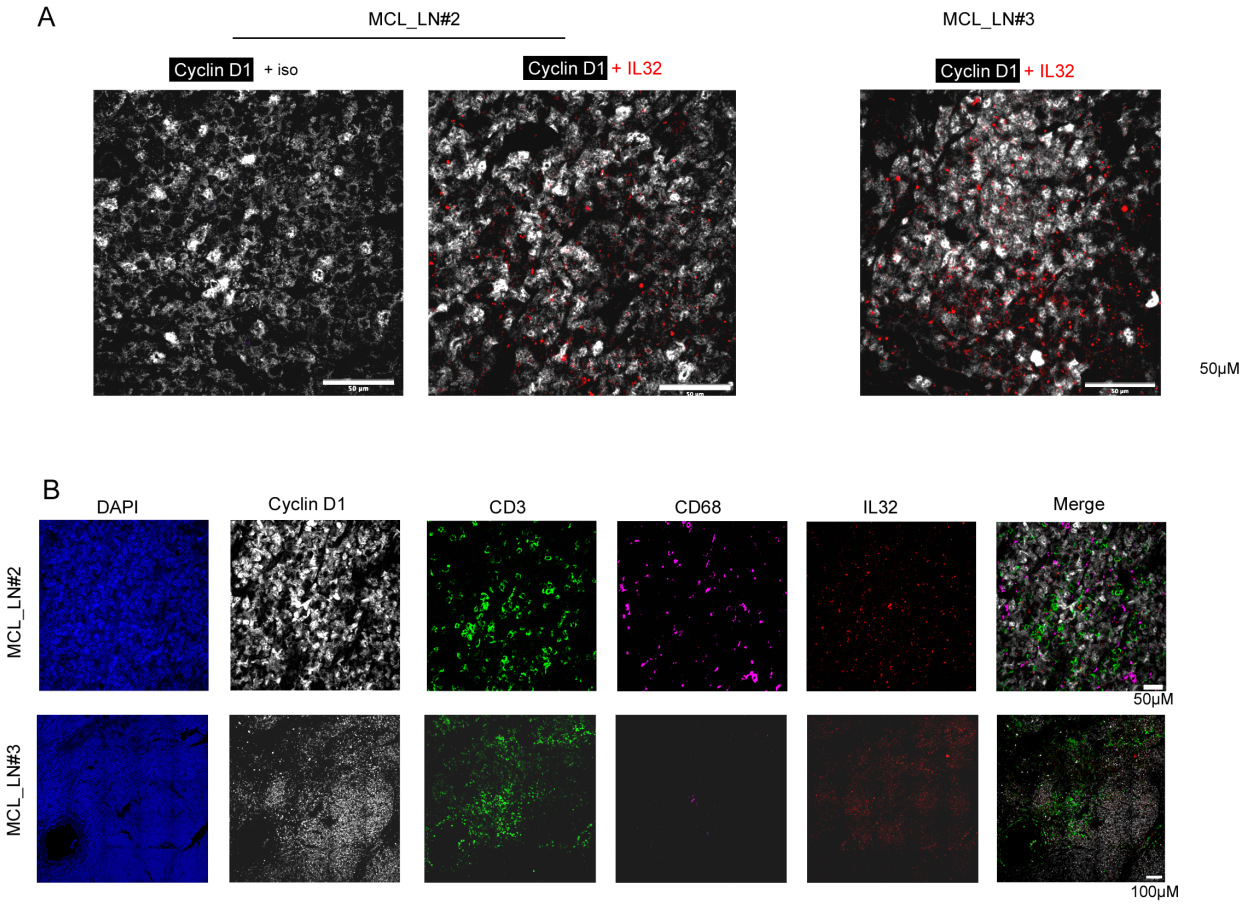

Supp. Fig. S9_ Individual stainings and controls of the multiplex immunohistochemestry experiment

Supplemental Figure Legends

Figure S1. Functional annotations and signature enrichment *in vivo* and *ex vivo*. (**A**) Top significantly modulated genes in LN compared with PB (GEP, log2Fc > 5; n= 22) and their localization by using the Compartments resources[10]. **(B)** KEGG pathway enrichment analysis of the *in vivo* LN upregulated gene set as represented in Figure 1B (n=4584 genes). The x-axis represents the normalized enrichment score (NES) as described by Joly et al. [11]. **(C)** Enrichment plots of the NFkB, NIK and BCR signatures (as described by Saba and colleagues[12]) or LN signature (100 most strongly upregulated genes in LN compared to PB MCL *in vivo*) analyzed using GSEA and reflecting the relevance of our *ex vivo* culture model previously described[9]. **(D)** KEGG pathway enrichment analysis of the "Tumor-specific" (n=1269 genes) and the "Shared with NBC" (n=1948 genes) gene sets as define in Figure 1B. The x-axis represents the normalized enrichment score (NES).

Figure S2. IL32 is expressed and induced by CD40L in MCL cell lines. (A) Concentration of IL32 protein determined by ELISA in the supernatant of NTS3, Z138, SP53, MINO and GRANTA cells. **(B)** *IL32* isoforms prediction by RNA-seq in Mino cells or primary NBC (n=2) and MCL cells (n=4) cultured or not on CD40L expressing cells for 7 days. **(C-D)** IL32 expression in MINO, NTS3 and REC-1 cells cultured on CD40L-expressing cells with or without growth factors (IL10, BAFF, IGF1, IL6) during 24h measured using RT-qPCR **(C)** or immunoblot **(D)**.

Figure S3. Alternative but not classical NFkB is involved in CD40L-induced IL32 expression. (A) Immunoblotting of indicated proteins in MCL cell lines in the presence or absence of the IKK inhibitor BMS-345541 (IKK-i, 5 µM, 6h) in Mino cells or NTS3 cells cultured on CD40L expressing cells. **(B)** Immunoblotting of indicated proteins in MINO cells treated with siRNA against *NFKB1* for 24 to 48h. **(C)** p52 protein expression in primary MCL cells (MCL14 and MCL15) from PB or LN was assessed.

Figure S4. Tumor-specific expression of IL32 is due to epigenetic regulations. (A) RT-qPCR analysis of *IL32* gene expression in Maver-1, UPN1 and SP53 cells treated or not with Decitabine (5'Aza) during 48h. **(B)** Left panel: Detailed locus specific bisulfite sequencing of *IL32* gene (promoter and CpG island) for indicated cells as described in the Methods. Black dots represent methylated CpG island. Mann-Whitney test. *p < 0.0261. Right panel: Locus specific bisulfite sequencing of promoter and CpG islands (CGI) of *IL32* gene for IL32 negative MCL cells (MAVER-1, Z138 and MCL cells (MCL12)) and IL32 positive cells (GRANTA, MINO and MCL cells (MCL5)). For all samples, PCR products were cloned and 8 were sequenced and analyzed as detailed in the Figure S4. Mann-Whitney test. ***p < 0.0002. **(C)** Locus specific bisulfite sequencing of the promoter of *IL32* gene in primary

$CD19^+$ $CD5^+$ NBC (n=1) or MCL (n=6) cells as in panel D. Mann-Whitney test. ****p < 0.0001. **(D)** Integration of the percentage of methylation analyzed by locus specific bisulfite sequencing of the promoter of *IL32* gene and the quantification of p52 and IL32 protein expression (immunoblotting) in NBC and MCL cells at D0 and after culture on CD40L-expressing cells for 7 days.

Figure S5. IL32 is coregulated with genes expressed by monocytes and T cells in MCL LN. (A) KEGG pathway enrichment analysis for the genes co-regulated with *IL32* gene in MCL cells. **(B)** IL32 top co-regulated genes in LN versus PB MCL cells were defined with the limma package. Genes related to macrophages (red circles) or T-cells (blue circles) functions are highlighted. **(C)** Comparison of the induced genes in both macrophages and monocytes treated with (rh)IL32β, as described in Figure 5 **(D)** Common KEGG pathway enrichment found in both macrophages and monocytes treated with (rh)IL32β, as described in Figure 5. The x-axis represents the normalized enrichment score (NES).

Figure S6. Secretome of IL32-stimulated monocytes and macrophages. (A) RT-qPCR analysis of *IL1A, IL1B, IL6, IL24, CXCL8, IL1B, IL32, BAFF* in monocytes or monocytes-derived macrophages cultured with (rh)IL32β for 24h or 48h respectively. Mann-Whitney test. **p < 0.005. **(B)** A pre-defined panel of soluble factors was measured by cytokine array (Proteome Profiler™, Human Cytokine Array, R&D Systems®) in the supernatant of monocytes-derived macrophages stimulated with CSF1 with or without (rh)IL32β for 3 days.

Figure S7. Generation of $IL32^{-/-}$ Mino and NTS3 cells through Crisp/Cas9 technology. (A) DNA sequencing of wild type (Cnt, upper panel) and $IL32^{-/-}$ (Cr#1, lower panel) Mino cells. Deletions are predicted for both alleles. Blue sequence represents the target sequence; red sequence represents the Pam sequence. **(B)** Immunoblotting of IL32 protein in wild type (Cnt) and $IL32^{-/-}$ MINO (Clone Cr#1) and NTS3 (Clones Cr#1 and Cr#2). **(C)** RT-qPCR analysis of *IL1A, IL1B, IL6, IL24, CXCL8, IL32 and BAFF* genes in monocytes cultured during 24h with wild type (-) or $IL32^{-/-}$ (Cr#1) CD40L-stimulated NTS3 supernatant.

Figure S8. BAFF-specific MCL cell rescue is dependent on alternative NFkB pathway. (A) Flow cytometry analysis of BAFFR expression in MCL cell lines (n=7) and in primary MCL cells from peripheral blood (PB, n=42) and bone marrow (BM, n=9). **(B)** Volcano-plot representation of whole transcriptome analysis (publicly available Affimetrix U133, see Methods) from MCL lymph nodes samples (LN, n=107) compared to MCL peripheral blood samples (PB, n=77) shown in figure 1A annotated for TNFSF13B and IL32. **(C)** Immunoblotting of NFkB pathway proteins in SP53, NTS3 and primary MCL cells (MCL13) cultured with BAFF (50 ng/mL) for 24h. **(D)** Percentage of cell rescue dependent on BAFF in

primary MCL (n=4) cultured with or without NIK inhibitor (NIK-i, 10 µM) for 7 days. Paired t test. *p < 0.05. **(E)** p52 protein expression in SP53 cells cultured with Mϕ-32 supernatant (s_Mϕ-32) for 16h with or without anti-BAFF neutralizing antibody (10 µg/mL) assessed by immunoblotting. **(F)** BclxL, MCL1, BCL2 and BCL2A1 gene expression analyzed by RT-qPCR in SP53 cells stimulated with or without BAFF (50 ng/ml) or CD40L during 6h. **(G)** Immunoblotting of alternative NFkB (p100 and p52) pathway and BclxL, MCL1 and A1 protein expression in SP53 and NTS3 cells cultured with or without BAFF (50 ng/ml) during 6 or 24h. **(H)** Immunoblotting of alternative NFkB (p100 and p52) pathway and BclxL, MCL1 and A1 protein expression in MCL11 and MCL13 MCL primary cells cultured with or without BAFF (50 ng/ml) during 6 or 24h and SP53 as a positive control (T+).

Figure S9. Individual stainings and controls on the Multiplex Immunohistochemistry experiment (A) Multiplex Immunohistochemistry on lymph nodes sections from 2 MCL patients (MCL_LN#2/3) for staining of Cyclin D1 (opal 570 ; white), and IL32 (opal 650 ; red) or Cyclin D1 (opal 570 ; white) and Rabbit Primary Antibody Isotype Control (opal 650 ; red). Scale bars, 50 µm. **(B)** Individual staining of Multiplex Immunohistochemistry on lymph nodes sections from 2 MCL patients: MCL_LN#2 (top panel, Scale bars, 50 µm) and MCL_LN#3 (bottom panel, Scale bar, 100 µm) for Cyclin D1 (opal 570 ; white), CD3 (opal 690 ; green), CD68 (opal 520 ; magenta), IL32 (opal 650 ; red). Nucleus is stained with Dapi.

Supplemental References

1. Maiga S, Brosseau C, Descamps G, et al. A simple flow cytometry-based barcode for routine authentication of multiple myeloma and mantle cell lymphoma cell lines. *Cytometry A*. 2015;87(4):285-288.
2. Martin M. Cutadapt removes adapter sequences from high-throughput sequencing reads. *EMBnet journal*. 2011;17(1):10-12.
3. Schmieder R, Edwards R. Quality control and preprocessing of metagenomic datasets. *Bioinformatics*. 2011;27(6):863-864.
4. Kim D, Pertea G, Trapnell C, Pimentel H, Kelley R, Salzberg SL. TopHat2: accurate alignment of transcriptomes in the presence of insertions, deletions and gene fusions. *Genome biology*. 2013;14(4):1-13.
5. Feng J, Meyer CA, Wang Q, Liu JS, Shirley Liu X, Zhang Y. GFOLD: a generalized fold change for ranking differentially expressed genes from RNA-seq data. *Bioinformatics*. 2012;28(21):2782-2788.
6. Hu Y, Liu Y, Mao X, et al. PennSeq: accurate isoform-specific gene expression quantification in RNA-Seq by modeling non-uniform read distribution. *Nucleic acids research*. 2014;42(3):e20-e20.
7. Magali S, Davide C, Stefan S, Alexander O, Tarjei S. Characterization of directed differentiation by high-throughput single-cell RNA-Seq. *BioRxiv*. 2014.
8. Love M, Anders S, Huber W. DESeq2 vignette. *Genome Biol doi*. 2016;110.
9. Chiron D, Bellanger C, Papin A, et al. Rational targeted therapies to overcome microenvironment-dependent expansion of mantle cell lymphoma. *Blood, The Journal of the American Society of Hematology*. 2016;128(24):2808-2818.
10. Binder JX, Pletscher-Frankild S, Tsafou K, et al. COMPARTMENTS: unification and visualization of protein subcellular localization evidence. *Database*. 2014;2014.
11. Joly JH, Lowry WE, Graham NA. Differential Gene Set Enrichment Analysis: A statistical approach to quantify the relative enrichment of two gene sets. *Bioinformatics*. 2020.
12. Saba NS, Liu D, Herman SE, et al. Pathogenic role of B-cell receptor signaling and canonical NF-κB activation in mantle cell lymphoma. *Blood, The Journal of the American Society of Hematology*. 2016;128(1):82-92.